

Figure 3. Temporal variation of simulated BaP concentrations at the Noto monitoring site with these source profiles.

Figure 4 shows the horizontal distributions of the simulated seasonal averaged particulate BaP concentrations and wind vectors near the surface. BaP was selected as a representative for the characterization of the total 9 PAHs because its high toxicity

causes a greater health impact. In winter (Figure 4a), high BaP concentrations were observed over a wide region in China, and we observed the transboundary transport of BaP from the Asian continent toward the Japanese islands. Northwestern or westerly winds prevailed over Northeast Asia during the observation period, which suggests that BaP is long-range transported from Northeast Asia to the Japanese islands. In spring (Figure 4b), the concentrations of BaP at the Noto monitoring site were decreased compared with those in winter under the weak westerly wind, suggesting that the transboundary transport was weakened. In contrast, as shown in Figure 4c, southerly and southwesterly winds prevailed over the Pacific Ocean under the Pacific High pressure system, which blocks transboundary transport of BaP from the Asian continent. In autumn (Figure 4d), the transition season from summer to winter, the transboundary transport of BaP is reinforced again.

These results suggest that the seasonal variation of BaP emission and the prevailing meteorological conditions strongly controlled transboundary transport in Northeast Asia. Under westerly winds, domestic coal, domestic biofuel, and other coal transformations, including coke production in China, were the dominant BaP sources at the Noto station, based on the source profile.

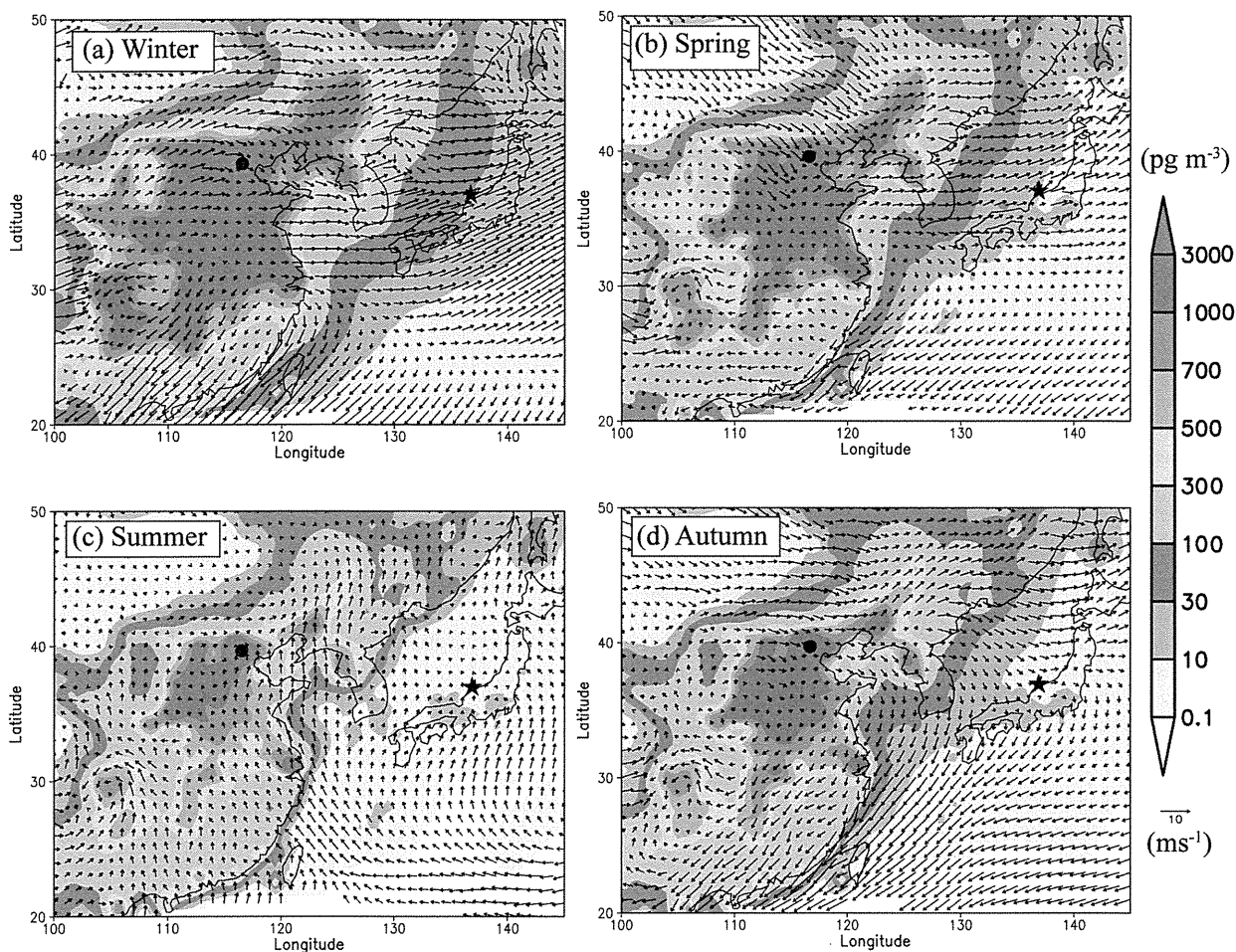


Figure 4. Spatial distributions of seasonal averaged BaP concentrations (a) Winter (December, January, and February), (b) Spring (March, April, May), (c) Summer (June, July, and August), and (d) Autumn (September, October, and November). The color scale is in units of pg m^{-3} . ● indicates the location of Beijing monitoring site, and ★ indicates the location of Noto monitoring site.

When westerly winds are weak in summer, relative contributions from other sources such as on-road mobile source were increased. The seasonal variation and the source profiles of the other PAH species were similar to those of BaP.

3.3. Uncertainty in Emission Factors for Emission Estimates. The majority of the emission factors that were used in this study were derived from the data from China. We have no specific emission factors for other Asian countries, with the exception of the on-road mobile sources in Japan and several data from Taiwan. In addition, the reported emission factors displayed large variations depending on the combustion processes, fuel composition, and oxygen supply. It is also expected that the emission factors of each category change rapidly as a result of technological innovations that have occurred over several decades, for instance, the elimination of dust. To set adequate emission factors, we conducted sensitivity calculations by changing the emission factors.

At first, the emission factor for each source was set to the same value, 1, for all of the Northeast Asian countries. Under this assumption, the seasonal variation (high in the winter and low in the summer) that was observed at Noto could not be simulated. In addition, the simulated concentrations in the summer at Noto were higher than those in the winter and spring. According to the trajectory analysis calculated for several years, most air masses arriving at Noto in summer were transported from the south or southwestern part of the Japanese islands.⁵⁴ The results of the sensitivity calculations with the high concentrations of the 9 PAHs in the summer at Noto suggest that the PAH emissions from the Japanese islands are too large. These results also imply that the same emission factor should not be used for all of the Northeast Asian countries. In fact, Wang et al. reported that the emission factors of 16 PAHs from on-road mobile sources in China were 100 times higher than those in Europe and the United States.³⁵ In this study, the emission factors of 9 PAHs that were derived from on-road mobile sources in China were approximately 100–1000 times greater than those in Japan.^{36,39} Based on these data, the emission factor of each source (with the exception of the on-road mobile sources) in the developed countries was set at $1/100$ of those in the developing countries in this study. Based on the country's Gross Domestic Product (GDP) per capita,⁵⁵ we arbitrarily divided the countries in Northeast Asia into two groups: developing countries (China, East Russia, Mongolia, and North Korea) and developed countries (Japan, South Korea, and Taiwan). As a result, the seasonal variation of the particulate PAH concentrations at Noto could be simulated well.

Second, we conducted sensitivity calculations by changing the emission factors of the domestic biofuel and domestic coal sources, which are the dominant contributors of particulate PAH emissions (SI Table S8). The range of BaP emission factors used in the data set varied from n.d. (not detected) to 88.8 mg kg^{-1} for domestic coal and $0.04\text{--}6.6 \text{ mg kg}^{-1}$ for domestic biofuel.^{2,20,26,27,42} For the emission factors of the other coal transformations source, which are also recognized as major PAH sources, we could not conduct the sensitivity calculations because there was only one source of data. Figure 5 shows the results of the sensitivity calculations for BaP at Noto using different emission factors (the maximum, median, and minimum values of the emission factors data set). The simulated concentrations using the median value of emission factors were reasonably consistent with the observed concentrations. Conversely, the concentrations simulated by using the

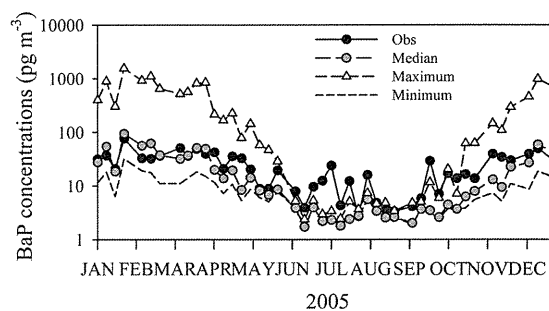


Figure 5. Sensitivity calculation for the simulated BaP concentrations at the Noto monitoring site using different emission factors. In the data set of emission factors for the domestic coal and domestic biofuel sources, the maximum, minimum, and median values were used for the sensitivity calculations.

maximum emission factor were approximately 100 times higher than the observed concentrations. In addition, it appears that the simulated concentrations were less than approximately $1/10$ of the measured concentrations when the minimum emission factor was used. It was reported that the emission factors of PAHs from coal combustion vary greatly depending on combustion conditions (temperature and oxygen supply associated with type of combustor), combustion efficiency, and component of coal.⁴¹ Regarding domestic biofuel combustion, the emission factors varied by several orders of magnitude due to many factors, including fuel moisture, combustion temperature, oxygen supply, and combustion place.⁴⁰ In fact, PAHs would be emitted under various combustion conditions and different fuel compositions. Because the results using the sensitivity calculations showed that the median value of emission factor predicted the observed BaP concentration well, we adopted the median value of the data set as the emission factor for each category.

■ ASSOCIATED CONTENT

📄 Supporting Information

Additional material as noted in the text. This material is available free of charge via the Internet at <http://pubs.acs.org>.

■ AUTHOR INFORMATION

Corresponding Author

*Phone: +81-25-263-0558; fax: +81-25-263-0567; e-mail: inomata@acap.asia.

Notes

The authors declare no competing financial interest.

■ ACKNOWLEDGMENTS

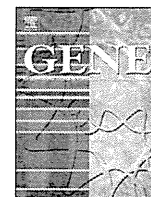
This research was financially supported by the Environment Research and Technology Development Fund (Project No. B-0905 and A-1101) of the Ministry of the Environment, Japan. We thank Dr. Kiriko Kashiwakura, Japan Automobile Research Institute, and Dr. Shinichiro Okayama, Nissan Motor Co. Ltd., for providing the emission factor data derived from automobiles in Japan.

■ REFERENCES

- (1) Agency for Toxic Substances and Disease Registry. *Toxicological Profile for Polycyclic Aromatic Hydrocarbons (PAHs)*; U.S. Department of Health and Human Service, Public Health Service: Atlanta, GA, 1995; www.atsdr.cdc.gov/ToxProfile/tp69.pdf.

- (2) Xu, S.; Liu, W.; Tao, S. Emission of polycyclic aromatic hydrocarbons in China. *Environ. Sci. Technol.* **2006**, *40*, 702–708, DOI: 10.1021/es0517062.
- (3) Zhang, Y. X.; Tao, S. Global atmospheric emission inventory of polycyclic aromatic hydrocarbons (PAHs) for 2004. *Atmos. Environ.* **2009**, *43*, 812–819, DOI: 10.1016/j.atmosenv.2008.10.050.
- (4) Ravindra, K.; Sokhi, R.; Grieken, R. V. Atmospheric polycyclic aromatic hydrocarbons: Source attribution, emission factors and regulation. *Atmos. Environ.* **2008**, *42*, 2895–2921, DOI: 10.1016/j.atmosenv.2007.12.010.
- (5) Tang, N.; Hattori, T.; Taga, R.; Igarashi, K.; Yang, X.; Tamura, K.; Kakimoto, H.; Mishukov, V. F.; Toriba, A.; Kizu, R.; Hayakawa, K. Polycyclic aromatic hydrocarbons and nitropolycyclic aromatic hydrocarbons in urban air particulates and their relationship to emission sources in the Pan-Japan Sea countries. *Atmos. Environ.* **2005**, *39*, 5817–5826, DOI: 10.1016/j.atmosenv.2005.06.018.
- (6) Yang, X.-Y.; Okada, Y.; Tang, N.; Matsunaga, S.; Tamura, K.; Lin, J.-M.; Kameda, T.; Toriba, A.; Hayakawa, K. Long-range transport of polycyclic aromatic hydrocarbons from China to Japan. *Environ. Environ.* **2007**, *41*, 2710–2718, DOI: 10.1016/j.atmosenv.2006.11.062.
- (7) Hattori, T.; Tang, N.; Tamura, K.; Hokoda, A.; Yang, X.; Igarashi, K.; Ohno, M.; Okada, Y.; Kameda, T.; Toriba, A.; Hayakawa, K. Particulate polycyclic aromatic hydrocarbons and their nitrated derivatives in three cities in Liaoning Province, China. *Environ. Forensics.* **2007**, *8*, 165–172, DOI: 10.1080/15275920601180701.
- (8) Zhang, Y.; Tao, S.; Shen, H.; Ma, J. Inhalation exposure to ambient polycyclic aromatic hydrocarbons and lung cancer risk of Chinese population. *Proc. Natl. Acad. Sci. U. S. A.* **2009**, *106*, 21063–21067, DOI: 10.1073/pnas.0905756106.
- (9) Gusev, A.; Dutchak, S.; Rozovskaya, O.; Shatalov, V.; Sokovykh, V.; Vulykh, N.; Aas, W.; Breivik, K. *Persistent Organic Pollutants in the environments*; EMEP Status Report 3/2011; Meteorological Synthesizing Centre-East: Moscow, Russia, 2011; www.msceast.org/reps/3_2011.pdf (accessed April 2, 2012).
- (10) Tsubulsky, V.; Sokolovsky, V.; Dutchak, S.; Shatalov, V. *MSC-E Contribution to the HM and POP Emission Inventories: Polycyclic Aromatic Hydrocarbon Emission Inventories and Emission Expert Estimates; Expert Estimates of Heavy Metal Emissions for some European Countries for 1980–98*; Technical Note 7/2001; Meteorological Synthesizing Centre-East: Moscow, 2001; www.msceast.org/index.php?option=com_content&view=article&id=27&Itemid=39#2001 (accessed April 2, 2012).
- (11) Pacyna, J. M.; Breivik, K.; Munch, J.; Fudala, J. European atmospheric emissions of selected persistent organic pollutants, 1970–1995. *Atmos. Environ.* **2003**, *37*, S119–S131, DOI: 10.1016/S1352-2310(03)00240-1.
- (12) U.S. Environmental Protection Agency. *1990 Emission inventory of Section 112(c) (6) Pollutants: Polycyclic Organic Matter (POM), TCDD, TCDF, PCBs, Hexachlorobenzene, Mercury, and Alkylated Lead*, Final Report, Emission Factor and Inventory Group (MD-14), Emissions Monitoring and Analysis Division; Visibility and Ecosystem Protection Group (MD-15), Air Quality Strategies and Standards Division; United States Environmental Protection Agency: Research Triangle Park, NC, 1998; www.epa.gov/ttn/atw/112c6/final2.pdf (accessed April 2, 2012).
- (13) Wenborn, M. J.; Coleman, P. J.; Passant, N. R.; Lymberidi, E.; Sully, J.; Weir, R. A. *Speciated PAH Inventory for the UK*, AEAT-3512/REMC/20459131/Issue 1; AEA Technology Environment: Oxford, UK, 1999; http://uk-air.defra.gov.uk/reports/cat08/0512011419_REPFIN_all_nov.pdf (accessed April 2, 2012).
- (14) Zhang, Y.; Dou, H.; Chang, B.; Wei, Z.; Qiu, W.; Liu, S.; Liu, W.; Tao, S. Emission of Polycyclic aromatic hydrocarbons from indoor straw burning and emission inventory updating in China. *Ann. N. Y. Acad. Sci.* **2008**, *1140*, 218–227, DOI: 10.1196/annals.1454.00.
- (15) Liu, S.; Tao, S.; Liu, W.; Liu, Y.; Dou, H.; Zhao, J.; Wang, L.; Wang, J.; Tian, Z.; Gao, Y. Atmospheric polycyclic aromatic hydrocarbons in north China: A winter-time study. *Environ. Sci. Technol.* **2007**, *41*, 8256–8261, DOI: 10.1021/es0716249.
- (16) Lang, C.; Tao, S.; Zhang, G.; Fu, J.; Simonich, S. Outflow of polycyclic aromatic hydrocarbons from Guangdong, Southern China. *Environ. Sci. Technol.* **2007**, *41*, 8370–8375, DOI: 10.1021/es071853v.
- (17) Zhang, Y.; Shen, H.; Tao, S.; Ma, J. Modeling the atmospheric transport and outflow of polycyclic aromatic hydrocarbons emitted from China. *Atmos. Environ.* **2011**, *45*, 2820–2827, DOI: 10.1016/j.atmosenv.2011.03.006.
- (18) Ohara, T.; Akimoto, H.; Kurokawa, J.; Horii, N.; Yamaji, K.; Yan, X.; Hayasaka, T. An Asian emission inventory of anthropogenic emission sources for the period 1980–2020. *Atmos. Chem. Phys.* **2007**, *7*, 4419–4444.
- (19) Kajino, M.; Inomata, Y.; Sato, K.; Kurokawa, J.; Ohara, T.; Tang, N.; Hayakawa, K.; Ueda, H. Modeling polycyclic aromatic hydrocarbons over Northeast Asia using MRI-PM/p. (in preparation).
- (20) U.S. Environmental Protection Agency. *Needs Assessment for U.S. EPA's Integrated Risk Information System*, EPA/635/R-02/004; National Center for Environmental Assessment, Office of Research and Development, United States Environmental Protection Agency: Washington, DC, 2003; www.epa.gov/iris/pdfs/iris_needs.pdf (accessed April 2, 2012).
- (21) Streets, D. G.; Bond, T. C.; Carmichael, G. R.; Fernandes, S. D.; Fu, Q.; He, D.; Klimont, Z.; Nelson, S. M.; Tsai, N. Y.; Wang, M. Q.; Woo, J.-H.; Yarber, K. F. An inventory of gaseous and primary aerosol emissions in Asia in the year 2000. *J. Geophys. Res.* **2003**, *108*, 8809, DOI: 10.1029/2002JD003093.
- (22) Carmichael, G. R.; Sakurai, T.; Streets, D.; Hozumi, Y.; Ueda, H.; Park, S. U.; Fung, C.; Han, Z.; Kajino, M.; Engardt, M.; Bennet, C.; Hayami, H.; Sartelet, K.; Holloway, T.; Wang, Z.; Kannari, A.; Fu, J.; Matsuda, K.; Thongboonchoo, N.; Amann, M. MICS-AsiaII: The model intercomparison study for Asia Phase II methodology and overview of findings. *Atmos. Environ.* **2008**, *42*, 3468–3490, DOI: 10.1016/j.atmosenv.2007.04.007.
- (23) Giglio, L.; Randerson, J. T.; Van der Werf, G. R.; Kasibhatla, P. S.; Collatz, G. J.; Morton, D. C.; DeFries, R. S. Assessing variability and long-term trends in burned area by merging multiple satellite fire products. *Biogeosci.* **2010**, *7*, 1171–1186, DOI: 10.5194/bg-7-1171-2010.
- (24) Yang, H.-H.; Lee, W.-J.; Chen, S.-J.; Lai, S.-O. PAH emission from various industrial stacks. *J. Hazard. Mater.* **1998**, *60*, 159–174.
- (25) Li, C.-T.; Mi, H.-H.; Lee, W.-J.; You, W.-C.; Wang, Y.-F. PAH emission from the industrial boilers. *J. Hazard. Mater.* **1999**, *A69*, 1–11.
- (26) Yan, J.-H.; You, X.-F.; Li, X.-D.; Ni, M.-J.; Yin, X.-F.; Cen, K.-F. Performance of PAHs emission from bituminous coal combustion. *J. Zhejiang Univ. Sci.* **2004**, *5*, 1554–1564, DOI: 10.1631/jzus.2004.1554.
- (27) Chen, Y.; Bi, X.; Mai, B.; Sheng, G.; Fu, J. Emission characterization of particulate/gases and size association for polycyclic aromatic hydrocarbons from residential coal combustion. *Fuel.* **2004**, *83*, 781–790, DOI: 10.1016/j.fuel.2003.11.003.
- (28) Chen, Y.; Sheng, G.; Bi, X.; Febg, Y.; Mai, B.; Fu, J. Emission factors for carbonaceous particles and polycyclic aromatic hydrocarbons from residential coal combustion in China. *Environ. Sci. Technol.* **2005**, *39*, 1861–1867, DOI: 10.1021/es0493650.
- (29) Oanh, N. T. K.; Albina, D. O.; Ping, L.; Wang, X. Emission of particulate matter and polycyclic aromatic hydrocarbons from select cookstove-fuel systems in Asia. *Biomass. Bioenergy.* **2005**, *28*, 579–590, DOI: 10.1016/j.biombioe.2005.01.003.
- (30) Kuo, C.-Y.; Lee, H.-S.; Lai, J.-H. Emission of polycyclic aromatic hydrocarbons and lead during Chinese mid-autumn festival. *Sci. Total Environ.* **2006**, *366*, 233–241, DOI: 10.1016/j.scitotenv.2005.08.006.
- (31) Chen, Y.-C.; Sigh, P.-H. Emission of polycyclic aromatic hydrocarbons on the combustion of liquid crystal display components. *J. Environ. Eng.* **2006**, *132*, 1028–1033, DOI: 10.1061/(ASCE)0733-9372(2006)132:9(1028).
- (32) Chen, S.-J.; Su, H.-B.; Chang, J.-E.; Lee, W.-J.; Huang, K.-L.; Hsieh, L.-T.; Huang, W.-J.; Lin, W.-Y.; Lin, C.-C. Emissions of polycyclic aromatic hydrocarbons (PAHs) from the pyrolysis of scrap

- tires. *Atmos. Environ.* **2007**, *41*, 1209–1220, DOI: 10.1016/j.atmosenv.2006.09.041.
- (33) Wang, H. L.; Zhuang, Y. H.; ZhengPin, H.; Cao, M.; Zhong, J. X.; Wang, X. K.; Oahn, N. T. K. Polycyclic aromatic hydrocarbons from rural household biomass burning in a typical Chinese village. *Sci. China. Ser. D-Earth Sci* **2008**, *51*, 1013–1020, DOI: 10.1007/s11430-008-0064-x.
- (34) Yuan, H.; Tao, S.; Li, B.; Lang, C.; Cao, J.; Coveney, R. M. Emission and outflow of polycyclic aromatic hydrocarbons from wildfires in China. *Atmos. Environ.* **2008**, *42*, 6828–6835, DOI: 10.1016/j.atmosenv.2008.05.033.
- (35) Wang, B.-G.; Lu, W.-M.; Zhou, Y.; Shao, M.; Zhang, Y.-H. Emission characteristic of PAHs composition in motor vehicles exhaust of city tunnel. *China Environ. Sci.* **2007**, *27*, 482–487.
- (36) Kashiwakura, K.; Sasaki, S.; Nakajima, T.; Sakamoto, K. Emissions of regulated and non-regulated air pollutants emitted from heavy-duty diesel vehicles and their emission tendencies. *J. Soc. Atmos. Environ.* **2008**, *43*, 67–78.
- (37) Chien, Y.-C.; Liang, C. P.; Shih, P. H. Emission of polycyclic aromatic hydrocarbons from the pyrolysis of liquid crystal wastes. *J. Hazard. Mater.* **2009**, *170*, 910–914, DOI: 10.1016/j.hazmat.2009.05.054.
- (38) Etiope, G.; Iversen, N.; Woodfield, M.; Winiwarter, W. *EMEP/EEA Air Pollutant Emission Inventory Guidebook 2009; EEA Technical Report, ISSN 1725-2237*; European Environment Agency: Copenhagen, 2009; www.eea.europa.eu/publications/emep-eea-emission-inventory-guidebook-2009 (accessed April 2, 2012).
- (39) Ho, K. F.; Ho, S. S. H.; Lee, S. C.; Cheng, Y.; Chow, J. C.; Watson, J. G.; Louie, P. K. K.; Tian, L. Emissions of gas- and particle-phase polycyclic aromatic hydrocarbons (PAHs) in the Shing Mun Tunnel, Hong Kong. *Atmos. Environ.* **2009**, *43*, 6343–6351, DOI: 10.1016/j.atmosenv.2009.09.025.
- (40) Lu, H.; Zhu, L.; Zhu, N. Polycyclic aromatic hydrocarbon emission from straw Burning and the influence of combustion parameters. *Atmos. Environ.* **2009**, *43*, 978–983, DOI: 10.1016/j.atmosenv.2008.10.022.
- (41) Liu, W. X.; Dou, H.; Wei, Z. C.; Chang, B.; Qiu, W. X.; Liu, Y.; Tao, S. Emission characteristics of polycyclic aromatic hydrocarbons from combustion of different residential coals in North China. *Sci. Total Environ.* **2009**, *407*, 1436–1446, DOI: 10.1016/j.scitotenv.2008.10.055.
- (42) Kashiwakura, K.; Sasaki, S.; Sakamoto, K. Emissions of regulated and non-regulated air pollutants emitted from gasoline vehicles and their emission tendencies. *J. Soc. Atmos. Environ.* **2009**, *44*, 102–116.
- (43) Shen, G.; Yang, Y.; Wang, W.; Tao, S.; Zhu, C.; Min, Y.; Xue, M.; Ding, J.; Wang, B.; Wang, R.; Shen, X.; Li, W.; Wang, X.; Russell, A. Emission factors of particulate matter and elemental carbon for crop residues and coals burned in typical household stoves in China. *Environ. Sci. Technol.* **2010**, *44*, 7157–7162, DOI: 10.1021/es101313y.
- (44) Cao, G. L.; Zhang, X. Y.; Wang, Y.; Zheng, F. Estimation of emissions from field burning of crop straw in China. *Chin. Sci. Bull.* **2008**, *53*, 784–790, DOI: 10.1017/s11434-008-0145-4.
- (45) Chan, D.; Song, T. Corrigendum to “Estimates of biomass burning emissions in Tropical Asia based on satellite-derived data” published in. *Atmos. Chem. Phys.* **2010**, *10*, 2335–2551.
- (46) Cao, G.; Zhang, X.; Zheng, F. Inventory of black carbon and organic carbon emissions from China. *Atmos. Environ.* **2006**, *40*, 6516–6527, DOI: 10.1016/j.atmosenv.2006.05.070.
- (47) Kajino, M.; Inomata, Y.; Sato, K.; Ueda, H.; Han, Z.; An, J.; Katata, G.; Deushi, M.; Maki, T.; Oshima, N.; Kurokawa, J.; Ohara, T.; Takami, A.; Hatakeyama, S. Development of an aerosol chemical transport model RAQM2 and predictionps of Northeast Asian aerosol mass, size, chemistry, and mixing type. *Atmos. Chem. Phys. Discuss.*, submitted.
- (48) An, J.; Ueda, H.; Wang, Z.; Matsuda, K.; Kajino, M.; Cheng, X. Simulations of monthly mean nitrate concentrations in precipitation over East Asia. *Atmos. Environ.* **2002**, *36*, 4159–4171.
- (49) Han, Z.; Ueda, H.; Sakurai, T. Model study on acidifying wet deposition in East Asia during wintertime. *Atmos. Environ.* **2006**, *40*, 2360–2373, DOI: 10.1016/j.atmosenv.2005.12.017.
- (50) Kajino, M.; Ueda, H.; Sato, K.; Sakurai, T. Spatial distribution of the source-receptor relationship of sulfur in Northeast Asia. *Atmos. Chem. Phys.* **2011**, *11*, 6475–6491, DOI: 10.5194/acp-11-6475-2011.
- (51) Gusev, A.; Mantseva, E.; Shatalov, V.; Strukov, B. *Regional Multicomponent Model MSCE-POP, Technical report, 5/2005 June*; Meteorological Synthesizing Center-East, 2005; www.msceast.org/index.php?option=com_content&view=article&id=27&Itemid=39#2005 (accessed April 2, 2012).
- (52) *ARW Version 3 Modeling System User's Guide*; National Center for Atmospheric Research: Boulder, CO, 2009; www.mmm.ucar.edu/wrf/users/docs/arw_v3.pdf (accessed April 2, 2012).
- (53) Hayakawa, K. Atmospheric Pollution and its countermeasure in East Asia from the viewpoint of polycyclic aromatic hydrocarbons. *J. Health Sci.* **2009**, *55*, 870–878.
- (54) Inomata, Y.; Chiba, M.; Igarashi, Y.; Aoyama, M.; Hirose, K. Seasonal and spatial variations of enhanced gamma dose rates derived from ²²²Rn progenies during precipitation in Japan. *Atmos. Environ.* **2007**, *41*, 8043–8057, DOI: 10.1016/j.atmosenv.2007.06.046.
- (55) *The World Factbook*; United States Central Intelligence Agency: Washington, DC, 2011; www.cia.gov/library/publications/the-world-factbook/rankorder/2004rank.html (accessed April 2, 2012).



Short Communication

Cloning of two members of the calcitonin-family receptors from stingray, *Dasyatis akajei*: Possible physiological roles of the calcitonin family in osmoregulation

Nobuo Suzuki ^{a,*}, Toshio Sekiguchi ^b, Honoo Satake ^b, Kanoko Kato ^c, Yudai Nishiyama ^c, Hideya Takahashi ^{c,d}, Janine A. Danks ^e, T. John Martin ^f, Atsuhiko Hattori ^g, Masaki Nakano ^g, Makiko Kakikawa ^h, Sotoshi Yamada ^h, Maho Ogoshi ^c, Susumu Hyodo ⁱ, Yoko Yamaguchi ⁱ, Vishwajit S. Chowdhury ^j, Kazuichi Hayakawa ^k, Hisayuki Funahashi ^l, Tatsuya Sakamoto ^c, Yuichi Sasayama ^a

^a Noto Marine Laboratory, Institute of Nature and Environmental Technology, Kanazawa University, Housu-gun, Ishikawa 927-0553, Japan

^b Bioorganic Research Institute, Suntory Foundation for Life Sciences, Osaka, 618-8503, Japan

^c Ushimado Marine Institute, Okayama University, Ushimado, Okayama 701-4303, Japan

^d Institute of Science and Technology, Niigata University, Niigata 950-2181, Japan

^e School of Medical Sciences, RMIT University, Bundoora 3083, Australia

^f St. Vincent's Institute of Medical Research, 41 Victoria Parade, Fitzroy 3065, Australia

^g Department of Biology, College of Liberal Arts and Sciences, Tokyo Medical and Dental University, Ichikawa-city, Chiba 272-0827, Japan

^h Institute of Nature and Environmental Technology, Kanazawa University, Kanazawa-city, Ishikawa 920-1192, Japan

ⁱ Atmosphere and Ocean Research Institute, University of Tokyo, Kashiwa-city, Chiba 277-8564 Japan

^j International Education Center, Faculty of Agriculture, Kyushu University, Fukuoka 812-8581, Japan

^k Faculty of Pharmaceutical Science, Institute of Medical, Pharmaceutical and Health Sciences, Kanazawa University, Kanazawa-city, Ishikawa 920-1192, Japan

^l Showa University, School of Medicine, Department of Anatomy, Shinagawa-ku, Tokyo 142-8555, Japan

ARTICLE INFO

Article history:

Accepted 4 March 2012

Available online 13 March 2012

Keywords:

Calcitonin

Calcitonin gene-related peptide

Tissue expression

Elasmobranch

ABSTRACT

In cartilaginous fish, two cDNAs encoding calcitonin-family receptors were isolated for the first time from the stingray brain. The open reading frame of one receptor cDNA coded a 525-amino acid protein. The amino acid identity of this receptor to human calcitonin-receptor-like receptor (CRLR) is 64.5%, frog CRLR is 64.7%, and flounder CRLR is 61.2% and this was higher than to human calcitonin receptor (CTR) (46.1%), frog CTR (54.7%), and flounder CTR (48.9%). We strongly suggested that this receptor is a ray CRLR based on phylogenetic analysis. In case of the second receptor, amino acid identity among CRLRs (human 50.5%, frog 50.7%, flounder 48.0%) and CTRs (human 43.2%, frog 49.1%, flounder 41.8%) was similar. From phylogenetic analysis of both CRLRs and CTRs, we believe that this receptor is ray CTR. The expression of ray CRLR mRNA was predominantly detected in the nervous system (brain) and vascular system (atrium, ventricle, and gill), which reflects the similar localization of CGRP in the nervous and vascular systems as mammals. It was observed that the second receptor was expressed in several tissues, namely cartilage, brain, pituitary gland, gill, atrium, ventricle, pancreas, spleen, liver, gall bladder, intestine, rectal gland, kidney, testis and ovary. This localization pattern was very similar to flounder CTR. Both receptor mRNAs were strongly expressed in the gill. This suggests that the calcitonin-family members are involved in the osmoregulation of stingray as this fish is known to be euryhaline. When a stingray was transferred to diluted seawater (20% seawater), the expression of both receptors significantly decreased in the gill. Similar results were obtained in the kidney of the stingray. Thus, our cloning and isolation of both receptors in the stingray will be helpful for elucidation of their physiological role(s) such as osmoregulation including calcium metabolism of cartilaginous fish.

© 2012 Elsevier B.V. All rights reserved.

Abbreviations: bp, base pair(s); cDNA, DNA complementary to RNA; CGRP, calcitonin gene-related peptide; CT, calcitonin; CTR, calcitonin receptor; CRLR, calcitonin-receptor-like receptor; mRNA, messenger RNA; PCR, polymerase chain reaction; RACE, rapid amplification of cDNA ends; RT-PCR, reverse transcription-polymerase chain reaction.

* Corresponding author at: Noto Marine Laboratory, Institute of Nature and Environmental Technology, Kanazawa University, Ogi, Noto-cho, Ishikawa 927-0553, Japan. Tel.: +81 768 74 1151; fax: +81 768 74 1644.

E-mail address: nobuos@staff.kanazawa-u.ac.jp (N. Suzuki).

1. Introduction

Calcitonin gene-related peptide (CGRP) is a 37 amino acid hormone whose mRNA is co-encoded with calcitonin (CT) mRNA on a single gene (Amara et al., 1982). In mammals, the mRNA synthesis of two hormones is controlled by tissue-specific alternative splicing; CGRP precursor mRNA is synthesized in the neural tissues; CT precursor mRNA is synthesized in the thyroidal C-cells (Rosenfeld et al., 1983). Since CGRP exists widely in the central nervous system

(Gibson et al., 1984; Rosenfeld et al., 1983), it is suggested that CGRP plays role as a neuromediator or neuromodulator (Lafont et al., 2007). In addition, CGRP is synthesized in the heart and blood vessels to control blood flow by its potent vasodilatory actions (Brain and Grant, 2004; Mulderry et al., 1985; Wimalawansa, 1997).

In teleosts, the presence of CGRP immunoreactive substances has been demonstrated in trout (Fouchereau-Peron et al., 1990). Jansz and Zandberg (1992) characterized the CGRP gene of salmon, suggesting that salmon CGRP is the product of the alternative splicing of the CT/CGRP gene, common to mammals. We also cloned a part of genomic DNA including the CGRP gene from flounder (*Paralichthys olivaceus*) and detected mRNA expression in the brain and heart (Suzuki et al., 2001), suggesting that CGRP acts as a neuropeptide and a vasodilator in fish as well as mammals, as CGRP immunoreactivity has been detected in the brain of small-spotted dogfish (Molist et al., 1995), and may be quite important in homeostasis in all fish including cartilaginous fish (Lafont et al., 2007). On the other hand, calcitonin receptor-like receptor (CRLR) functions to a receptor for CGRP when it is co-expressed with RAMP1 (Husmann et al., 2000; McLatchie et al., 1998; Sexton et al., 2001). The distribution and expression analysis of CRLR under various physiological and environmental conditions could contribute to the understanding of physiological functions of CGRP in cartilaginous fish.

To study the physiological role of CGRP in cartilaginous fish, the full coding region of CRLR was sequenced from the brain of stingray and the mRNA expression in the various tissues was analyzed. In the process of CRLR cloning, a second member of the calcitonin-family receptors was isolated and cloned. Based on the data of multiple alignment, phylogenetic analysis and tissue distribution pattern, it is apparent that this receptor is equivalent to the stingray calcitonin receptor (CTR). In addition, it was found that the expression of two receptors was decreased in the gill and kidney when the rays were transferred to diluted seawater. Thus, this is the first study that identifies two members of calcitonin-family receptors in cartilaginous fish and indicates the possible physiological roles of CT and CGRP in the osmoregulation of stingray.

2. Materials and methods

2.1. Animals

The brain of male stingray (*Dasyatis akajei*) was used for PCR amplification. Male and female stingrays were used for the analysis of tissue-specific expression and adaptation in seawater. The original concentration of seawater (100%) and diluted seawater (20%) were

used for this study. The animals were anesthetized with ethyl 3-amino-benzoate, methanesulfonic acid salt (Sigma-Aldrich Inc., MO, USA) and then dissected for tissue preparation.

All experimental procedures were conducted in accordance with the Guide for the Care and Use of Laboratory Animals prepared by Kanazawa University.

2.2. PCR amplification

Total RNAs were prepared using a total RNA isolation kit (Nippon Gene, Tokyo, Japan) from the brains of stingray. RT-PCR was performed using Oligotex-dT 30 Super (Takara, Kusatsu, Japan) as an oligo dT primer to prevent genomic DNA contamination (Suzuki et al., 1997). The PCR primers were designed at the well-conserved region of the mammalian CRLR and CTR cDNA sequences (Fig. 1). The primer sequences were 5'-1:GYAAYMGXACXTGGGAYGG, 5'-2:GAYTAYTTYCCXGAYTTYGA, 3'-1:CCYTCRCAXARCATCCARAA, and 3'-2:CATCCARAARTARTTRCA (Suzuki et al., 2000). The 1st and the nested-PCR (1st PCR: 5'-1/3'-1 primer set; 2nd PCR: 5'-2/3'-2 primer set) were performed using a *Taq* polymerase and an additional buffer (Takara Bio Inc., Otsu, Japan). The PCR parameters were 35 cycles of 96 °C for 30 s, 45 °C for 1 min, and 72 °C for 2 min. The sequencing of the PCR products of the expected length (422 bp) was performed by Dragon Genomics Center, Takara Bio Inc. (Mie, Japan).

2.3. RACE amplification of receptors cDNAs in stingray

Total RNA (1 µg) was obtained from the stingray brain. The complete sequences of the two receptors were obtained by 5'- and 3'-RACE method using a kit 5' RACE System, Version 2.0 and 3' RACE System for Rapid Amplification of cDNA Ends, respectively (Invitrogen, CA, USA). The primer locations for two receptors were described in supplementary figures. RACE was performed using the respective gene-specific primer and the primer of adaptor sequences in the kit. The products were sequenced on an ABI PRISM 3130 sequencer (Applied Biosystems, CA, USA) using BigDye terminators.

2.4. Expression analysis

Total RNAs were prepared from the cartilage, brain, pituitary gland, gill atrium, ventricle, pancreas, spleen, liver, gall bladder, intestine, rectal gland, kidney, and testis of male stingray, as well as the ovary of female stingray using a total RNA isolation kit (Nippon Gene). RT-PCR was performed using the primer set (CRLR 5': AGACTTCGATCCATCAGA, CRLR 3': AGTCAATGCTGTCTTTA, CTR-like

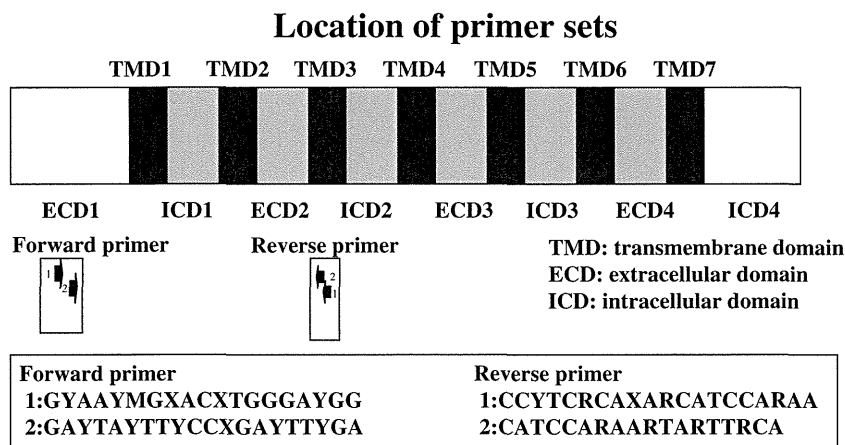


Fig. 1. Location and sequence of primers. The CRLR and CTR molecules have four extracellular domains (Ecd) 1–4, seven transmembrane domains (Tmd 1–7), and for intracellular domains (Icd 1–4). The PCR primers were designed to the highly conserved region of the mammalian CRLR and CTR cDNA sequences.

5': CACGAAAAGGTCACC, CTR-like 3': AGTGAACAAAGAGTAATAT). The conditions for PCR amplification were 40 cycles of denaturation for 0.5 min at 96 °C, annealing for 1 min at 60 °C, and extension for 2 min at 72 °C, followed by a single cycle at 72 °C for 30 min. In case of the β -actin cDNA (AB675482), the amplification using a primer set (5': TTGGCAATGAGCGATTGAGA; 3': CACAGGATTCCATACCCAA-GAAA) were consisted of 25 cycles of denaturation for 0.5 min at 96 °C, annealing for 1 min at 60 °C, and extension for 2 min at 72 °C, followed by a single cycle at 72 °C for 15 min. The PCR products were analyzed on 2.5% NuSive GTG agarose gel (FMC Bioproducts, ME, USA) and stained with ethidium bromide.

2.5. Phylogenetic analysis

The amino acid sequences were aligned using the CLUSTAL program (Higgins and Sharp, 1988). After removing gaps, the verified alignments were used to construct phylogenetic trees. The trees were calculated using MEGA program based on the neighbor-joining method (Kumar et al., 2001; Saitou and Nei, 1987). The sequences used were as follows: Human-CRLR, NP_005786; Pig-CRLR, Q867C1; Dog-CRLR, XP_545560; Mouse-CRLR, NP_061252; Xenopus-CRLR, NP_001016893; Fugu-CRLR2, BAE45313; Salmon-CRLR, CAD48406; Flounder-CRLR, AB035314; Fugu-CRLR1, BAE45312; Flounder-CTR, AB035315; Chicken-CTR, XP_425985; Bullfrog-CTR, Q28DX2; Fugu-CTR, BAE76018; Medaka-CTR, AAI19273; Pig-CTR, AAA31023; Mouse-CTR, AAI19273; Human-CTR, NP_001733; Dog-CTR, XP_539423; Ascidian-CTR, BAI63096; Human-CRHR1, NP_004373.

2.6. Analysis of the mRNA expression of both ray CRLR and CTR-like receptors in the gill and kidney after transfer to diluted seawater

Seawater adapted-stingrays ($n=8$, both sexes) were gradually transferred into diluted seawater. In the first day, the stingrays were transferred to 80% seawater and then kept for 6 hours followed by putting them into 60% seawater for remaining of the day. In the next day, the stingrays were kept in 40% seawater for 6 hours, and then transferred into 20% seawater. After keeping the stingrays in 20% seawater for 12 hours, the stingrays were anesthetized with ethyl 3-aminobenzoate, methanesulfonic acid salt (Sigma-Aldrich). The gill and kidney were collected from stingray under proper anesthetic condition. Also, the seawater-adapted stingrays ($n=8$, both sexes) were anesthetized with ethyl 3-aminobenzoate, methanesulfonic acid salt (Sigma-Aldrich). The gill and kidney were removed from the seawater stingrays.

Total RNA was prepared using a total RNA isolation kit for fibrous tissue and complementary DNA synthesis was performed (RNase Easy Fibrous Mini-Kit, Qiagen GmbH, Hilden, Germany). The real-time PCR amplification was analyzed with a Bio-Rad iCycler (Bio-Rad, Hercules, CA) using the primers for CRLR (5': GGA-GAAGCTAAAGACAGCATTGACT; 3': CAGCAGCGAAGCCACTGATA') and for CTR-like (5': GGAAAAGGTCACCAAGATTTGC; 3': AGTC-CATGTTCCGGTTGCTCTCT). The annealing temperature in the amplification of both CRLR and CTR-like cDNAs was 63 °C. The amplified PCR products have been verified by sequencing to confirm its sequences. The detailed conditions of PCR were described in our previous study (Takahashi et al., 2007). The CRLR and CTR-like mRNA levels were normalized to the β -actin mRNA level measured by above described primer set (5': TTGGCAATGAGCGATTGAGA; 3': CACAGGATTCCATACCCAAAGAAA).

2.7. Statistical analysis

Real-time PCR was performed and the data were analyzed using the Student's *t*-test. The significance level was $P<0.05$.

3. Results and discussion

3.1. PCR amplification of two receptors in the brain of stingray

Sequence analysis indicated that two types of cDNA fragments are amplified by PCR primer sets at the conserved regions of mammalian CRLR and CTR cDNA sequences. One cDNA fragment (422 bp) had high identity to flounder CRLR (73.4%) and human CRLR (81.3%) and to a lesser extent to flounder CTR (53.9%) and human CTR (56.3%). The second cDNA (422 bp) had high identity to both CRLR (to human 57.0%; to flounder 48.3%) and CTR (to human 59.4%; to flounder 63.3%). Thus, we believe that two receptors belong to the calcitonin-family receptors.

3.2. RACE cloning and sequencing of two calcitonin-family receptors

By RACE cloning, the full sequences of the two calcitonin-family receptors were determined. The open reading frame of one receptor cDNA coded a 525-amino acid protein (see Supplementary data). The amino acid identity of this receptor to CRLR was highest with human CRLR (64.5%), frog (64.7%), and flounder (61.2%) and this was higher than the CTR of human (46.1%), frog (54.7%), or flounder (48.9%). This strongly suggested that the obtained cDNA encodes CRLR in stingray.

The amino acid identity of the second stingray receptor (see Supplementary data) was similar to CRLRs (human 50.5%, frog 50.7%, flounder 48.0%) and CTRs of other species (human 43.2%, frog 49.1%, flounder 41.8%). After alignment of flounder CRLR, flounder CTR, human CRLR, human CTR, and two stingray receptors, three potential sites (Asn-X-Ser/Thr) for N-linked glycosylation, which are conserved in mammalian CRLR and CTR, were identified in stingray receptors before the first putative transmembrane domain. Furthermore, 12 cysteines were conserved among CRLRs, CTRs, and stingray receptors. These glycosylation sites and cysteines are suggested to be important for ligand binding (Ho et al., 1999; Qi et al., 1997). Using BLAST against the DDBJ/NCBI protein database, furthermore, we confirmed that the sequences are most similar to CRLR and CTR. Thus, we concluded that two receptors belong to the calcitonin-family receptors.

3.3. Phylogenetic analysis of calcitonin-family receptors

The phylogenetic tree was determined for the known calcitonin-family receptors together with stingray receptors (see Supplementary data). As a result, the stingray receptors were located with CRLR and CTR in other animals. The first stingray receptor branched from teleost CRLR and composed of a clade of mammalian and xenopus CRLR. This result strongly supports that the amino acid sequence was that of stingray CRLR (ray CRLR). The second stingray receptor co-located with flounder CTR and was placed between the CRLRs clade and the non-mammalian CTRs clade (see Supplementary data).

We previously reported amino acid sequences of both CT and CGRP in flounder (Suzuki et al., 2001). The amino acid sequence of flounder CT was more similar to teleosts (78–100%), salamander (81%), reptiles (84%), and chicken (84%) than those of stingray (72%) and frogs (56–78%), and it is largely different from that of mammals (31–50%). However, the predicted amino acid sequence of flounder CGRP was more conserved than CT among vertebrates and showed 78%, 78%, 78%, 81%, and 73–78% identity to salmon, cod, frog, chicken, and mammalian CGRPs, respectively. Among vertebrates, CGRP is a well-conserved molecule during evolution while CT is quite varied. Corresponding to sequence changes in ligand (CT), the receptor (CTR) seems to be varied largely. Thus, it is highly likely that the second receptor is the stingray equivalent of CTR (ray CTR-like).

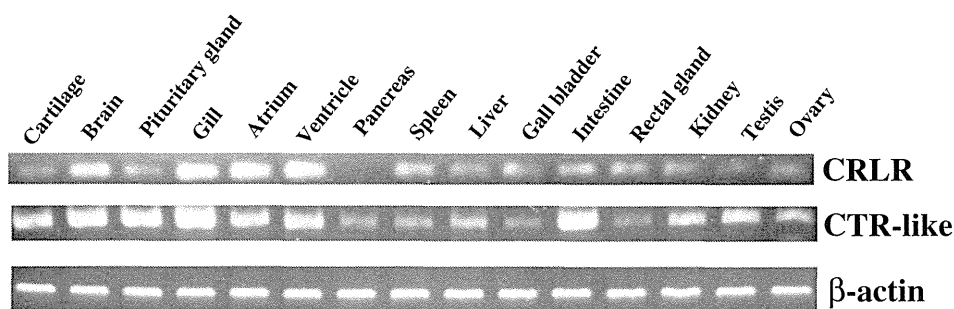


Fig. 2. Tissue specific expression of ray CRLR and ray CTR-like mRNAs by RT-PCR. After PCR amplification, the PCR products were analyzed on 2.5% NuSieve GTG agarose gel (FMC Bioproducts, ME, USA) and stained with ethidium bromide.

3.4. Expression of ray CRLR and ray CTR-like mRNAs in different tissues

Specific PCR products of ray CRLR mRNA were amplified from brain, gill, atrium and ventricle and detected in cartilage, pituitary gland, spleen, liver, gall-bladder, intestine, rectal gland, kidney, testis and ovary (Fig. 2). Pancreas did not show any expression with the present conditions (Fig. 2). The ray CRLR mRNA expression was found in brain, heart and intestine and this was the same as seen in mammals (Eysselein et al., 1991; Poyner, 1992), suggesting similar functions in those tissues. In spleen, relatively high expression of ray CRLR was detected. Arlot-Bonnemains et al. (1991) reported that CGRP-specific binding in trout tissues is high in the spleen although the function has not yet been elucidated. In the early development of gut in zebrafish, the number of nerve cell bodies and fibers gradually increased and CGRP was detected in these nerve cells (Olsson et al., 2008). In another study, cod CGRP (10^{-9} – 10^{-7} M) inhibited the motility of spontaneously active ring preparations from the cod intestine (Shahbazi et al., 1998) suggesting that CGRP plays a role in fish gut development and physiology. The localization of CGRP in the stingray gut suggests that CGRP may have significant roles in its gut.

Recently, involvement of CGRP in the outgrowth of the gubernaculum has been noted, and it has been suggested to play a role in testicular descent in mammals (Chan et al., 2009). CGRP released from the genitofemoral nerve causes maximal mitosis in the gubernacular bulb of mammals (Chan et al., 2009). In stingray, this hormone may involve in testicular development that regulates the balance between cell proliferation and apoptosis.

Specific PCR products of ray CTR-like mRNA were amplified from cartilage, brain, pituitary gland, gill, atrium, ventricle, pancreas, spleen, liver, gall bladder, intestine, rectal gland, kidney, testis, and ovary (Fig. 2). In the cartilage of stingray, we detected ray CTR-like mRNA expression. It has been reported that CT acts on mammalian cartilage and promotes synthesis (Karsdal et al., 2006; Sondergaard et al., 2006). In the stingray, thus, CT may function to the growth of cartilage. CT-immunoreactive cells were found in the intestine of goldfish and appeared to control absorption of nutrients (Okuda et al., 1999). Therefore, the presence of ray CTR-like mRNA in intestine corresponds well with this physiological role of CT in fish. Previously mRNA expression of salmon CTR was detected in brain and pituitary gland and this was consistent with another study in mammalian tissues (Azria, 1989) where it was suggested that CT might act as a neurotransmitter.

In female sharks, it had been shown that plasma CT levels were elevated during reproductive periods (Nichols et al., 2003). We previously reported that estrogen-specific-binding and estrogen receptor mRNA were present in the stingray ultimobranchial gland (CT secreting organ in sub-mammalian vertebrates) (Yamamoto et al., 1996). The possible involvement of CT in stingray reproductive physiology is implied because of the presence of this receptor in the ovary and testis of stingray in the present study.

Ray CRLR and ray CTR-like mRNAs were found to be expressed in the excretory organs such as gill, kidney and rectal gland. As this fish is euryhaline (de Vlaming and Sage, 1973; Evans et al., 2010; Janech et al., 2003) and CGRP functions to osmoregulation in teleosts (Lafont et al., 2007; Lamharzi and Fouchereau-Peron, 1996; Suzuki

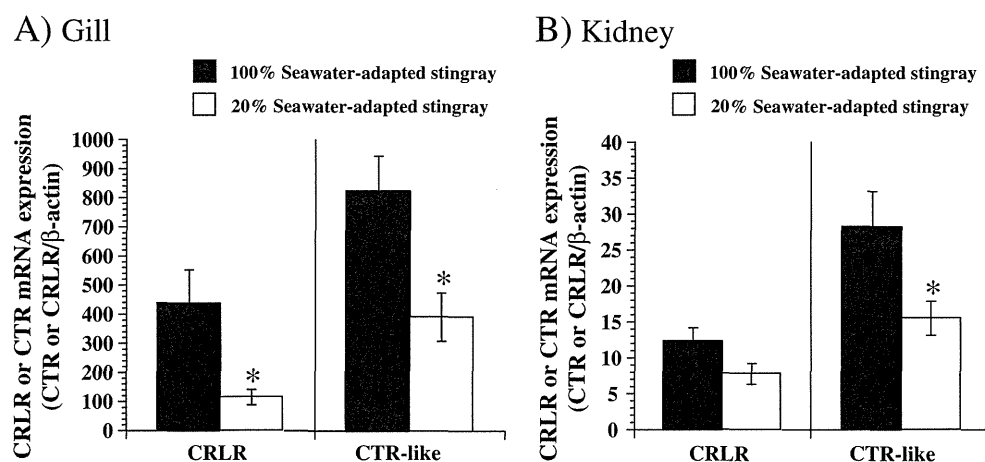


Fig. 3. Changes in mRNA expression of both ray CRLR and CTR-like receptors in the gill (A) and kidney (B) when transferred to diluted (20%) seawater. * indicates statistically significant difference at $P < 0.05$ from the values in the control. The data were expressed as mean \pm SEM ($n = 8$).

et al., 2002), we examined ray CRLR and ray CTR-like mRNA expression in the gill and kidney when stingrays were transferred to the diluted seawater.

3.5. Changes in mRNA expression of both ray CRLR and CTR-like receptors in the gill and kidney when transferred to diluted seawater

The results are shown in Fig. 3. The ray CTR-like mRNA expression in the gill and kidney was higher than the ray CRLR mRNA. These results coincided with the tissue specific expressions (Fig. 2). When stingrays were transferred to the diluted seawater (20% seawater), both receptors mRNA expression significantly decreased in the gill. Similar results were obtained in the stingray kidney. When rainbow trout were adapted to seawater, their plasma CGRP levels and CGRP binding sites in the gill increased (Lamharzi and Fouchereau-Peron, 1996). Similarly when flounder were moved from seawater to freshwater, CRLR mRNA expression decreased (Suzuki et al., 2002). Thus, CGRP may play a role in osmoregulation in teleosts (Lafont et al., 2007).

Interestingly, the plasma level of CT did not change when freshwater adapted eels were moved to 100% seawater (Suzuki et al., 1999). This was reflected in the study where the flounder were transferred from seawater to freshwater and CTR mRNA expression in the gill did not alter (Suzuki et al., 2002). Therefore, CT may play a role in osmoregulation in cartilaginous fish and not in teleosts, as CT has some functions in osmoregulation as the CTR-like mRNA expression in both stingray gill and kidney was decreased when the fish were transferred from seawater to freshwater. Further study is required to elucidate the possible roles of CT and CGPR in cartilaginous fish.

3.6. Conclusions

- (1) cDNA encoding CRLR was cloned from the stingray brain. Tissue-expression analysis, using RT-PCR, indicated that ray CRLR mRNA was detected mainly in the nervous system (brain) and vascular system (atrium, ventricle, and gill), indicating that CGRP may play roles in the nervous and vascular systems as it does in mammals.
- (2) Another receptor cDNA was cloned from the brain of stingray. Based on the data of multiple alignments, phylogenetic analysis and tissue distribution pattern, this receptor is CTR equivalent in stingray.
- (3) When stingray transferred to the diluted seawater (20% seawater), mRNA expression of both receptors was significantly decreased in the stingray gill. Similar results were obtained in the kidney. Thus, identification of two members of the calcitonin-family receptors in the stingray will assist in the elucidation of the physiological roles of these receptors and their ligands in cartilaginous fish.

Acknowledgments

This study was supported in part by grants to N.S. (Grant-in-Aid for Scientific Research (C) No. 21500404 by JSPS; Grant-in-Aid for Space Utilization by Japan Aerospace Exploration Agency), to A.H. (Grant-in-Aid for Scientific Research (C) No. 21570062 by JSPS), to T.S. (Grant-in-Aid for Scientific Research (C) No. 22570065 by JSPS), to M.O. (Grant-in-Aid for Encouragement of Scientists No. 22870020 by JSPS), and to K.H. [the Environment Research and Technology Development Fund (B-0905) by the Ministry of the Environment in Japan; Health and Labor Sciences Research Grants of Ministry of Health, Labor and Welfare, Japan; Grant-in-Aid for Scientific Research (B) No. 21390034 by JSPS]. This work was carried out in part as a joint-research in Japanese Association for Marine Biology (JAMBIO).

Appendix A. Supplementary Data

Supplementary data to this article can be found online at doi:10.1016/j.gene.2012.03.042.

References

- Amara, S.G., Jonas, V., Rosenfeld, M.G., Ong, E.S., Evans, R.M., 1982. Alternative RNA processing in calcitonin gene expression generates mRNAs encoding different polypeptide products. *Nature* 298, 240–244.
- Arlot-Bonnemains, Y., Fouchereau-Peron, M., Jullienne, A., Milhaud, G., Moukhtar, M.S., 1991. Binding sites of calcitonin gene related peptide (CGRP) to trout tissues. *Neuropeptides* 20, 181–186.
- Azria, M., 1989. *The Calcitonins: Physiology and Pharmacology*. Karger, Basel.
- Brain, S.D., Grant, A.D., 2004. Vascular actions of calcitonin gene-related peptide and adrenomedullin. *Physiol. Rev.* 84, 903–934.
- Chan, J.J., Farmer, P.J., Southwell, B.R., Sourial, M., Hutson, J.M., 2009. Calcitonin gene-related peptide is a survival factor, inhibiting apoptosis in neonatal rat gubernaculum *in vitro*. *J. Pediatr. Surg.* 44, 1497–1501.
- De Vlaming, V.L., Sage, M., 1973. Osmoregulation in the euryhaline elasmobranch, *Dasyatis Sabina*. *Comp. Biochem. Physiol.* 45A, 31–44.
- Evans, A.N., Henning, T., Gelsleichter, J., Nunez, B.S., 2010. Molecular classification of an elasmobranch angiotensin receptor: quantification of angiotensin receptor and natriuretic peptide receptor mRNAs in saltwater and freshwater populations of the Atlantic stingray. *Comp. Biochem. Physiol.* 157B, 423–431.
- Eysselein, V.E., et al., 1991. Structural characterization of calcitonin gene-related peptide purified from rabbit intestine. *Peptides* 12, 289–295.
- Fouchereau-Peron, M., Arlot-Bonnemains, Y., Taboulet, J., Milhaud, G., Moukhtar, M.S., 1990. Distribution of calcitonin gene-related peptide and calcitonin-like immunoreactivity in trout. *Regul. Pept.* 27, 171–179.
- Gibson, S.J., et al., 1984. Calcitonin gene-related peptide immunoreactivity in the spinal cord of man and of eight other species. *J. Neurosci.* 4, 3101–3111.
- Higgins, D.G., Sharp, P.M., 1988. CLUSTAL: a package for performing multiple sequence alignment on a microcomputer. *Gene* 73, 237–244.
- Ho, H.H., Gilbert, M.T., Nussenzveig, D.R., Gershengorn, M.C., 1999. Glycosylation is important for binding to human calcitonin receptors. *Biochemistry* 38, 1866–1872.
- Husmann, K., Sexton, P.M., Fischer, J.A., Born, W., 2000. Mouse receptor-activity-modifying proteins 1, -2, and -3: amino acid sequence, expression and function. *Mol. Cell. Endocrinol.* 162, 35–43.
- Janech, M.G., et al., 2003. Molecular and functional characterization of a urea transporter from the kidney of the Atlantic stingray. *Am. J. Physiol. Renal Physiol.* 284, F996–F1005.
- Jansz, H.S., Zandberg, J., 1992. Identification and partial characterization of the salmon calcitonin/CGRP gene by polymerase chain reaction. *Ann. N. Y. Acad. Sci.* 657, 63–69.
- Karsdal, M.A., et al., 2006. Calcitonin is involved in cartilage homeostasis: is calcitonin a treatment for OA? *Osteoarthritis Cartilage* 14, 617–624.
- Kumar, S., Tamara, K., Jakobsen, I.B., Nei, M., 2001. MEGA2: molecular evolutionary genetics analysis software. *Bioinformatics* 17, 1244–1245.
- Lafont, A.-G., Dufour, S., Fouchereau-Peron, M., 2007. Evolution of the CT/CGRP family: comparative study with new data from models of teleosts, the eel, and cephalopod molluscs, the cuttlefish and the nautilus. *Gen. Comp. Endocrinol.* 153, 155–169.
- Lamharzi, N., Fouchereau-Peron, M., 1996. Adaptation of rainbow trout to seawater: changes in calcitonin gene-related peptide levels are associated with an increase in hormone-receptor interaction in gill membranes. *Gen. Comp. Endocrinol.* 102, 274–280.
- McLatchie, L.M., et al., 1998. RAMPs regulate the transport and ligand specificity of the calcitonin-receptor-like receptor. *Nature* 393, 333–339.
- Molist, P., Rodriguez-Moldes, I., Batten, T.F.C., Anadon, R., 1995. Distribution of calcitonin gene-related peptide-like immunoreactivity in the brain of the small-spotted dogfish, *Scyliorhinus canicula* L. *J. Comp. Neurol.* 352, 335–350.
- Mulderry, P.K., et al., 1985. Calcitonin gene-related peptide in cardiovascular tissues of the rat. *Neuroscience* 14, 947–954.
- Nichols, S., Gelsleichter, J., Manire, C.A., Cailliet, G.M., 2003. Calcitonin-like immunoreactivity in serum and tissues of the bonnethead shark, *Sphyrna tiburo*. *J. Exp. Zool. A Comp. Exp. Biol.* 298, 150–161.
- Okuda, R., Sasyama, Y., Suzuki, N., Kambegawa, A., Srivastav, A.K., 1999. Calcitonin cells in the intestine of goldfish and a comparison of the number of cells among saline-fed, soup-fed, or high Ca soup-fed fishes. *Gen. Comp. Endocrinol.* 113, 267–273.
- Olsson, C., Holmberg, A., Holmgren, S., 2008. Development of enteric and vagal innervation of the zebrafish (*Danio rerio*) gut. *J. Comp. Neurol.* 508, 756–770.
- Poyner, D.R., 1992. Calcitonin gene-related peptide: multiple actions, multiple receptors. *Pharmacol. Ther.* 56, 23–51.
- Qi, L.J., Leung, A.T., Xiong, Y., Marx, K.A., Abou-Samra, A.-B., 1997. Extracellular cysteines of the corticotropin-releasing factor receptor are critical for ligand interaction. *Biochemistry* 36, 12442–12448.
- Rosenfeld, M.G., et al., 1983. Production of a novel neuropeptide encoded by the calcitonin gene via tissue-specific RNA processing. *Nature* 304, 129–135.
- Saitou, N., Nei, M., 1987. The neighbor-joining method: a new method for reconstructing phylogenetic trees. *Mol. Biol. Evol.* 4, 406–425.
- Sexton, P.M., Albiston, A., Morfis, M., Tilakaratne, N., 2001. Receptor activity modifying proteins. *Cell. Signal.* 13, 73–83.

- Shahbazi, F., Karila, P., Olsson, C., Holmgren, S., Conlon, J.M., Jensen, J., 1998. Primary structure, distribution, and effects on motility of CGRP in the intestine of the cod *Gadus morhua*. *Am. J. Physiol. Regul. Integr. Comp. Physiol.* 275, R19–R28.
- Sondergaard, B.C., et al., 2006. Calcitonin directly attenuates collagen type II degradation by inhibition of matrix metalloproteinase expression and activity in articular chondrocytes. *Osteoarthritis Cartilage* 14, 759–768.
- Suzuki, N., Eguchi, C., Hirai, T., Sasayama, Y., 1997. Nucleotide sequences of reptile calcitonins: their high homology to chicken calcitonin. *Zool. Sci.* 14, 833–836.
- Suzuki, N., Suzuki, D., Sasayama, Y., Srivastav, A.K., Kambegawa, A., Asahina, K., 1999. Plasma calcium and calcitonin levels in eels fed a high calcium solution or transferred to seawater. *Gen. Comp. Endocrinol.* 114, 324–329.
- Suzuki, N., Suzuki, T., Kurokawa, T., 2000. Cloning of a calcitonin gene-related peptide receptor and a novel calcitonin receptor-like receptor from the gill of flounder, *Paralichthys olivaceus*. *Gene* 244, 81–88.
- Suzuki, N., Suzuki, T., Kurokawa, T., 2001. Cloning of a calcitonin gene-related peptide from genomic DNA and its mRNA expression in flounder, *Paralichthys olivaceus*. *Peptides* 22, 1435–1438.
- Suzuki, N., Suzuki, T., Kurokawa, T., 2002. Possible involvement of calcitonin gene-related peptide in seawater adaptation of flounder: expression analysis of its receptor mRNA in the gill. *Fish. Sci.* 68, 425–429.
- Takahashi, H., et al., 2007. Prolactin receptor and proliferating/apoptotic cells in esophagus of the Mozambique tilapia (*Oreochromis mossambicus*) in fresh water and in seawater. *Gen. Comp. Endocrinol.* 152, 326–331.
- Wimalawansa, S.J., 1997. Amylin, calcitonin gene-related peptide, calcitonin, and adrenomedullin: a peptide superfamily. *Crit. Rev. Neurobiol.* 11, 167–239.
- Yamamoto, K., Suzuki, N., Takahashi, N., Sasayama, Y., Kikuyama, S., 1996. Estrogen receptors in the stingray (*Dasyatis akajei*) ultimobranchial gland. *Gen. Comp. Endocrinol.* 101, 107–114.



Original Full Length Article

Expression of osteoblastic and osteoclastic genes during spontaneous regeneration and autotransplantation of goldfish scale: A new tool to study intramembranous bone regeneration

Thiparpa Aime Thamamongood^{a,b}, Ryo Furuya^{c,b}, Shunsuke Fukuba^{d,b}, Masahisa Nakamura^c, Nobuo Suzuki^e, Atsuhiko Hattori^{b,*}

^a Undergraduate School of Medicine, Tokyo Medical and Dental University, Bunkyo-ku, Tokyo 113-8549, Japan

^b Department of Biology, College of Liberal Arts and Sciences, Tokyo Medical and Dental University, Ichikawa-shi, Chiba 272-0827, Japan

^c Department of Biology, Faculty of Education and Integrated Arts and Sciences, Waseda University, Shinjuku-ku, Tokyo 162-8480, Japan

^d Undergraduate School of Dentistry, Tokyo Medical and Dental University, Bunkyo-ku, Tokyo 113-8549, Japan

^e Noto Marine Laboratory, Institute of Nature and Environmental Technology, Kanazawa University, Noto-cho, Ishikawa 927-0553, Japan

ARTICLE INFO

Article history:

Received 7 December 2011

Revised 6 March 2012

Accepted 18 March 2012

Available online 29 March 2012

Edited by: T. Jack Martin

Keywords:

Osteoblastic genes

Osteoclastic genes

Teleost scale regeneration

Scale autotransplantation

Intramembranous bone regeneration

Cell-to-cell contact

ABSTRACT

Complementary DNA of osteoblast-specific genes (*dlx5*, *runx2a*, *runx2b*, *osterix*, *RANKL*, type I collagen, *ALP*, and *osteocalcin*) was cloned from goldfish (*Carassius auratus*) scale. Messenger RNA expressions were analyzed during spontaneous scale regeneration. *Dlx5* had an early peak of expression on day 7, whereas *osterix* was constantly expressed during days 7–21. *Runx2*, a major osteoblastic transcription factor in mammalian bone, did not show any significant expression. The expressions of two functional genes, type I collagen and *ALP*, continually increased after day 7, while that of *osteocalcin* increased on day 14. As for osteoclastic markers, in addition to the cloning of two functional genes, *TRAP* and *cathepsin K*, in our previous study, we here cloned the transcription factor *NFATc1* to use as an early osteoclastic marker. Using these bone markers, we investigate the signal key that controls the onset of scale resorption and regeneration by performing intra-scale-pocket autotransplantation of five groups of modified scales, namely, 1) methanol-fixed scale, 2) proteinase K-treated cell-free scale, 3) polarity reversal (upside-down) scale, 4) U-shape trimmed scale, and 5) circular-hole perforated scale. In this autotransplantation, each ontogenic scale was pulled out, modified, and then re-inserted into the same scale pocket. At post-transplant, inside the pockets of all modified transplant groups, new regenerating scales formed, attaching to the ongoing resorbed transplants. Autotransplantation of methanol-fixed scale, proteinase K-treated cell-free scale, and polarity reversal (upside-down) scale triggered scale resorption and scale regeneration. These two processes of scale resorption and regeneration occurred in accordance with osteoclastic and osteoblastic marker gene expressions. These results were microscopically confirmed using *TRAP* and *ALP* staining. Regarding the autotransplantation of U-shape trimmed and circular-hole perforated scales, new scales regenerated and grew at the trimmed/perforated part of each transplant, while scale resorption occurred apparently only around the trimmed/perforated area. In contrast, no scale resorption or regeneration was detected in sham transplantations. Our finding suggests that loss of correct cell-to-cell contact between the scale-pocket lining cells and the scale cortex cells is the key to switch on the onset of scale resorption and regeneration. Overall, the present study shows that goldfish scale regeneration shares similarities in gene expression with intramembranous bone regeneration. Improved understanding of goldfish scale regeneration will help elucidate the process of intramembranous bone regeneration and make goldfish scale a possible new tool to study bone regeneration.

© 2012 Elsevier Inc. All rights reserved.

Introduction

Teleost fish, a fish of a large group (division Teleostei) that comprises most bony fishes, has two main types of scales, cycloid and ctenoid.

Cycloid scales are scales with a smooth surface. Fish such as goldfish and carp have cycloid scales. Ctenoid scales have tiny points on their surface and are found on fish such as bass and perch. Teleost scale has been shown to be a good model for studying bone metabolism [1–4]. It contains calcified tissue consisting of osteoblasts, osteoclasts, and bone matrix protein. The scale of teleost shares many characteristics with mammalian membrane bone. We previously reported morphological similarity between scale regeneration and membrane bone osteogenesis [2]. In the mentioned study, scale

* Corresponding author at: Department of Biology, College of Liberal Arts and Sciences, Tokyo Medical and Dental University, 2-8-30 Kounodai, Ichikawa, Chiba 272-0827, Japan. Tel./fax: +81 473 00 7126.

E-mail address: ahattori.las@tmd.ac.jp (A. Hattori).

osteoblast appearance and activity were discussed by comparing to those in developmental study of mammalian membrane bone [5–9]. For osteoclast, we reported that scale osteoclasts create a ruffled border which is rich in mitochondria to increase the surface area interface for bone resorption. Mature osteoclasts in scales are multinucleated and express tartrate-resistant acid phosphatase (TRAP) and cathepsin K [1]. Recently, it was found that scale osteoblasts and osteoclasts are capable of responding to parathyroid hormone 1 (1–34) [10].

In fish skeletal tissue, a number of osteoblastic markers have been detected: alkaline phosphatase (ALP) [11]; runt related transcription factor 2 (runx2) [12]; and receptor activator of the NF- κ B ligand (RANKL) [13]. In the scale of teleost, type I collagen is present in goldfish scale (*Carrasius auratus*) [14]. Osterix expression has been observed in the scales of medaka (*Oryzias latipes*) [15]. Osteocalcin, a marker for mature bone matrix producing cells in mammals as well as teleost species [16–18], has been purified from scales of bluegill (*Lepomis macrochirus*) [19]. In zebrafish, osteocalcin mRNAs have been localized in all mineralized tissues during and after calcification, including bone and calcified cartilage of branchial arches [16]; however, to date, no research has been conducted to examine the pattern expression of osteocalcin during scale regeneration. Dlx5 (distal less homeobox5) stimulates osteoblast differentiation in mammals [20]. A number of *in vitro* studies have shown that dlx5 mediates BMP2-induced runx2 and osterix expressions [21,22]. In teleost, dlx5 is expressed during the developmental process of visceral skeleton [23] and medial fin fold [24] in zebrafish. Nevertheless, to the best of our knowledge, dlx5 expression in teleost scale has not been studied.

During scale regeneration, scale pocket-lining cells are capable of differentiating into scale-forming and scale-regenerating cells [25]. This significant osteoblastic potential is common to that of bone periosteum. The periosteum contains osteogenic cells in the cambial layer and fibroblasts in the fibrous layer [26–29]. Sire [30] observed that, when a scale is experimentally pulled off, the scale-forming cells are removed with the dermis, but the scale pocket-lining cells are not damaged. Furthermore, epidermal fragments remain at the posterior edge of each scale pocket. The restoration of the normal scale pattern in regenerated scales depends on the presence of the scale pocket-lining cells, and, if they are damaged, abnormal scalation patterns and abnormal scales are produced [31].

To elucidate osteoblastic actions during scale regeneration, we cloned eight osteoblast-specific genes, dlx5, runx2a, runx2b, osterix, RANKL, type I collagen, ALP, and osteocalcin cDNAs, from goldfish (*C. auratus*) ontogenic scale and analyzed their mRNA expression patterns in regenerating scales. This is the first report of the full coding sequence of osterix, ALP, and osteocalcin molecules in goldfish. In addition, we previously demonstrated that TRAP and cathK mRNA are expressed in multinucleated osteoclasts of goldfish scale [1]. In this study, we succeeded in cloning the nuclear factor of activated T-cells, cytoplasmic 1 (NFATc1), an early osteoclastic marker which has been previously reported in mammalian bone [32].

Furthermore, to study the factor that controls the onset of scale resorption and regeneration, we conducted intra-pocket autotransplantation of five groups of modified scales, *i.e.*, 1) methanol-fixed scale, 2) proteinase K-treated cell-free scale, 3) polarity reversal (upside-down) scale, 4) U-shape trimmed scale, and 5) circular-hole perforated scale. TRAP and ALP staining were performed to investigate scale resorption and scale regeneration. Additionally, in the present study, we analyzed osteoclastic and osteoblastic marker gene expression for the first two groups (methanol-fixed and proteinase K-treated transplants) and compared them with those in sham transplantations and ontogenic scales.

The ability of cementless joint replacement implants, dental implants, and rigid internal fracture fixation devices to restore function depends in part upon intramembranous bone regeneration [33]. Future advances in implant fixation and fracture repair may benefit from an improved understanding of intramembranous bone regeneration.

Nevertheless, gene expression patterns during intramembranous bone regeneration are poorly understood. To date, a method such as mechanical ablation of the marrow cavity is a convenient model of intramembranous bone regeneration [34–38]. However, one of the weak points of this model is that it requires that the animal be sacrificed to observe tissue regeneration; thus, results from each regeneration stage cannot be obtained from the same animal. The results from our current study show that bone-related genes during scale regeneration show almost the same expression trends as those in bone marrow ablation-induced intramembranous bone regeneration [39–41]. Therefore, we consider goldfish scale as a possible new tool for studying the process of intramembranous bone regeneration.

Materials and methods

Animals

Goldfish (*C. auratus*) were purchased from a commercial source (Higashikawa Fish Farm, Yamatokoriyama, Japan) and kept under normal laboratory conditions before the start of experiments. All experimental procedures were conducted in accordance with Tokyo Medical and Dental University's Guideline for the Care and Use of Laboratory Animals.

Complementary DNA cloning

Ontogenic scales were collected from male goldfish (body length = 14.8 ± 2.7 cm) under anesthesia with MS-222 (Sigma). Total RNA was isolated from the collected scales by using ISOGEN (Nippon Gene) and kept at -80 °C until the start of experiments. RNA was reverse-transcribed to cDNA using SuperScript III (Invitrogen). The resulting cDNA was served as a template for touchdown PCR amplification using degenerate primers. Information on cDNA nucleotide sequences and mature protein amino acid sequences of dlx5, osterix, runx2a (MASNS and MRIPV isoforms [42]), runx2b (MASNS and MRIPV isoforms [42]), type I collagen, osteocalcin, and NFATc1 of teleosts was obtained from GenBank through the web pages of the National Center of Biotechnology Institution. PCR products of the length of interest were gel-purified and cloned into PCR2.1 vector (Invitrogen) and Ligation high (TOYOBO). The sequence analysis was performed by using a BigDye Terminator v3.1 Cycle Sequencing Kit (Applied Biosystems) and an automated DNA sequencer (ABI Prism 3100-Avant, Applied Biosystems).

Rapid amplification of cDNA ends (RACE)

We obtained 5' and 3' ends of osterix, ALP, and osteocalcin by RACE. Template cDNA was prepared by using a Super SMART PCR cDNA synthesis kit (Clontech). RACE was performed by using the adapter primer supplied in the cDNA synthesis kit and specific primers for cloned PCR fragment sequences.

Amino acid sequence analysis

Amino acid sequence alignments were performed with the Clustal W multiple sequence alignment program available on the website of the DNA Data Bank of Japan (DDBJ). The amino acid identity of each predicted polypeptide was compared with *Xenopus laevis*, *Mus musculus*, and *Homo sapiens*.

Analysis of osteoblastic marker mRNA expression in spontaneously regenerated scales

Scales on the left side of the body were removed from goldfish (N = 15) after anesthetization with MS-222. On days 7, 14, and 21, goldfish were anesthetized with MS-222 again, and both regenerating (left side) and remaining ontogenic (right side) scales were collected.

Total RNA was isolated from collected scales by using ISOGEN and treated with DNase I. Two micrograms of total RNA was reverse-transcribed at 50 °C for 60 min and 70 °C for 15 min in 40 µl of a mixture containing 2 µl of SuperScript III, 10 mM dNTPs, 2 µl of RNase inhibitor, and 20 µM oligo-(dT). Quantitative real-time PCR analysis of *dlx5*, *runx2a*, *runx2b*, *osterix*, *RANKL*, type I collagen, ALP, osteocalcin, and β -actin (GenBank ID: AB039726) was performed by using the SYBR® Premix Ex Taq™ (TaKaRa Bio Inc.) and Mx3000 P® QPCR System (Stratagene). Real-time PCR was carried out with 1 µg of the first-strand mixture in 10 µl of a PCR mixture containing 5 µl of SYBR® Premix Ex Taq™, 0.2 µl of the ROX reference dye, and 0.2 µl of each gene-specific primer (Table 1). The conditions for PCR amplification consisted of 10 s of initial denaturation at 95 °C followed by 40 cycles of denaturation at 95 °C for 30 s, annealing and extension at 65 °C for 30 s, and a single cycle for dissociation curve analysis (95 °C for 5 s, 55 °C for 30 s, and 95 °C for 5 s). To control for differences in starting mRNA conditions, the mRNA levels of β -actin were used as an internal standard. The relative values of target mRNA expression were calculated from the target threshold cycle values and β -actin threshold cycle values using standard curves.

Scale modification and autotransplantation

Ontogenic scales were removed from goldfish under anesthesia with MS-222 and divided into five equal groups for five different modifications, including 1) methanol fixation, 2) proteinase K treatment, 3) scale polarity reversal (upside-down), 4) U-shape trimming, and 5) circular-hole perforation. In the first group, scales were immersed in a 99.8% methanol solution for 5 min at room temperature.

Table 1
Primer sequences for quantitative real-time reverse-transcription PCR.

| Primers | Nucleotide sequences (5'-3') |
|-------------------------------------|------------------------------|
| <i>Dlx5</i> | |
| <i>Dlx5</i> -F | CCGAGCCCAGAGTGAGGAT |
| <i>Dlx5</i> -R | GAAGAGCTGGCGCTTCCAG |
| <i>Osterix</i> | |
| <i>Osterix</i> -F | GACTGCCTGACCAGCGTCAA |
| <i>Osterix</i> -R | GAGGCCACCAAGCCTCTCCAA |
| <i>Runx2a</i> ^a | |
| <i>Runx2a</i> -F | TCCCACTGGAGGTGCAACAA |
| <i>Runx2a</i> -R | GGGTGGTGAGGTGGATGGAG |
| <i>Runx2b</i> ^a | |
| <i>Runx2b</i> -F | GACAGCAGCAGCAGGACAGC |
| <i>Runx2b</i> -R | TGAGAAGGCAACACCGAGCA |
| <i>RANKL</i> | |
| <i>RANKL</i> -F | GCGCTTACCTGCGGAATCATATC |
| <i>RANKL</i> -R | AAGTGCAACAGAATCGCCACAC |
| Type I collagen | |
| Type I collagen-F | TGCAACACAGGATGCCATCAA |
| Type I collagen-R | ATGAGGCGCAGGAAGGTGAG |
| Alkaline phosphatase | |
| ALP-F | TGGACACAGCGGTGAGGAAA |
| ALP-R | GTGGGCATATGCTGCACTCG |
| Osteocalcin | |
| Osteocalcin-F | ATGCCTGAGCGCAGGTCTTC |
| Osteocalcin-R | CACAGGCCAGGTTTGCTTCA |
| NFATc1 | |
| NFATc1-F | CTGTCTGCGTTTTGGGAAAG |
| NFATc1-R | GATGCTGGTGTGCTGCTAACC |
| Tartrate-resistant acid phosphatase | |
| TRAP-F | TGCTGGACACTGTGCTGCTG |
| TRAP-R | GGAACCTGGTTTTGCGGTGTCG |
| CathepsinK | |
| CathK-F | TGGGAGGGCTGGAAACTCAC |
| CathK-R | CATGAGCCGATGAACCTTG |
| β -actin | |
| β -actin-F | CGAGCGTGGCTACAGCTTCA |
| β -actin-R | GCCCGTCAGGAGCTCATAG |

^a *Runx2a* and *runx2b* primers were determined from the highly conserved area of MASNS and MRIPV isoforms.

In the second group, scales were immersed in a 0.05% proteinase K solution for 20 min. Using a microscope, we confirmed that this proteinase K-treated procedure caused the scales to become cell-free. Both groups were then repeatedly rinsed in distilled water and autotransplanted to their original scale pockets under anesthesia. In the third group, scales were upside-down autotransplanted immediately after being pulled off. In the fourth group, each scale was U-shape-trimmed at the rostral part using a 5 mm-diameter hole punch. In the fifth group, one circular hole was made at the central part of scale using a 1 mm-diameter hole punch. The goal of each modification was 1) methanol fixation was conducted to make all cells on the scales non-living cells; 2) Proteinase K treatment was conducted to make scales to be entirely cell-free by detaching all cells; 3) Scale polarity reversal (upside-down) was carried out to disrupt the correct cell-to-cell contact between the scale pocket and the scale cortex; and 4) U-shape trimming and circular-hole perforation were conducted to partially eliminate cell-to-cell communication between the scale pocket and the scale cortex. As a control, other scales were pulled out and immediately re-inserted in their original positions (sham autotransplant).

Histological observations of scale resorption and new scale formation

After autotransplantation, goldfish (N=25) were anesthetized again, and transplanted scales were collected from each animal on days 3, 5, 10, and 15 for modified groups 1–3 (methanol-fixed scales, proteinase K-treated scales, and polarity reversal (upside-down) scales), and, on day 10, for modified groups 4–5 (U-shape trimmed scales and circular-hole perforated scales). These scales were immersed in 10% formaldehyde in a 0.05 M cacodylate buffer (pH 7.4) for 10 min at room temperature, rinsed in distilled water, and incubated at 37 °C in the dark for 1 h in a tartrate-resistant acid phosphatase (TRAP) staining solution [1,10,43]. An assay for TRAP consisted of naphthol AS-BI phosphate solution, diazotized fast garnet GBC base solution, sodium nitrite solution, acetate solution (pH 5.2), and 10 mM L(+)-tartrate solution. ALP staining was performed separately by using NBT/BCIP stock solution at 35 °C for 30 min [43]. After staining, they were observed under an optical microscope.

Measurements of osteoclastic and osteoblastic marker mRNA levels in methanol-fixed scales and proteinase K-treated scales at post-autotransplantation

Autotransplantation of methanol-fixed scales and proteinase K-treated cell-free scales was conducted in goldfish (N=15) along with sham autotransplantations. On post-autotransplant day 3 and day 15, the autotransplanted scales and the remaining ontogenic scales were collected. Total RNA was isolated, and real-time RT-PCR analysis of NFATc1, TRAP, cathK, RANKL, *dlx5*, *osterix*, type I collagen, osteocalcin, and β -actin was performed as described above. Each gene-specific primer is shown in Table 1.

Statistical analysis

All results are expressed as the mean \pm SEM. Statistical significance was assessed by one-way ANOVA followed by the Bonferroni method. The data of the relative expression amount of genes in autotransplanted scales at post-autotransplantation were analyzed after taking logarithms.

Results

Cloning of osteoblastic and osteoclastic marker cDNA from the scale of goldfish

RT-PCR amplification using degenerate primers was successfully employed to amplify the fragments of *dlx5*, *runx2a* (MASNS and MRIPV isoforms), *runx2b* (MASNS and MRIPV isoforms), *osterix*,

RANKL, type I collagen, ALP, osteocalcin, and NFATc1 shown in Table 2. Osterix, ALP, and osteocalcin fragments were subjected to 5' and 3' RACE, and then the sequence of the resulting 2064 bp, 2391 bp, and 469 bp cDNA was determined. The nucleotide sequence data of goldfish *dlx5*, *runx2a* (MASNS), *runx2a* (MRIPV), *runx2b* (MASNS), *runx2b* (MRIPV), *osterix*, RANKL, type I collagen, ALP, osteocalcin, and NFATc1 cDNA has been submitted to the DDBJ/EMBL/GenBank DNA database under each GenBank ID listed in Table 2. The comparison of the amino acid sequences of goldfish *dlx5*, *runx2a* (MASNS), *runx2a* (MRIPV), *runx2b* (MASNS), *runx2b* (MRIPV), *osterix*, RANKL, type I collagen, ALP, osteocalcin, and NFATc1 with *Danio rerio*, *X. laevis*, *M. musculus*, and *H. sapiens* is shown in Table 2. RANKL and osteocalcin have low degrees of identity with *X. laevis*, *M. musculus*, and *H. sapiens*. The other genes have greater than 80% homology with *D. rerio* and greater than 50% homology with other vertebrates. Concerning the full sequences, for *osterix*, residues of three zinc finger structures, a putative nuclear localization signal, and a repetitive motif, GSSPL, are conserved with the specific protein7 (Sp7)/*osterix* of humans and rodents [44], while the proline-rich domain shares low homology. For ALP, metal ligand sites and residues that interact with substrate phosphate [45] are conserved, whereas the N and C terminals have low homology to humans, rodents, and amphibians. For osteocalcin, the Gla region including the two Cys [46] and the teleost's unique highly conserved sequence near the C-terminal, AAYXAYGP(I/P) [47], are highly conserved. Other regions of osteocalcin share low homology with tetrapods.

Expression pattern of osteoblastic markers in the spontaneous regenerating scale

We found that osteoblastic markers were expressed in the regenerating scale and that the expression of *dlx5*, *osterix*, type I collagen, ALP, and osteocalcin mRNAs increased remarkably during scale regeneration, although that of *runx2a* and *runx2b* mRNA was not higher than that of ontogenic scale (Figs. 1A–B). On day 7, *Dlx5* mRNA expression reached the peak level and declined (Fig. 1C), whereas *osterix* mRNA expression increased and persisted (Fig. 1D). Two functional genes of osteoblasts, type I collagen and ALP, were expressed since the early stage of scale regeneration (Figs. 1E–F), while osteocalcin mRNA expression was increased later on day 14 (Fig. 1G).

Table 2

Amplified fragment length and comparison of amino acid sequences of goldfish *dlx5*, *runx2a* (MASNS and MRIPV), *runx2b* (MASNS and MRIPV), *osterix*, RANKL, type I collagen, ALP, osteocalcin, and NFATc1 to *Danio rerio*, *Xenopus laevis*, *Mus musculus*, and *Homo sapiens*.

| Amplified fragment | Length (bp) | Amino acid sequence homology (%) | | | |
|-----------------------|----------------|-----------------------------------|--------------------------------------|------------------------------------|------------------------------------|
| | | <i>Danio rerio</i> UniProt ID: | <i>Xenopus laevis</i> UniProt ID: | <i>Mus musculus</i> UniProt ID: | <i>Homo sapiens</i> UniProt ID: |
| <i>Dlx5</i> | 411 (partial) | 96.06% | 90.00% | 80.71% | 80.00% |
| GenBank ID: AB685218 | | Q5XJL9 | Q6GLJ3 | P70396 | P56178 |
| <i>Runx2a</i> (MASNS) | 884 (partial) | 95.28% | 69.31% | 61.65% | 63.25% |
| GenBank ID: AB274884 | | Q6U1J2 | A1YIX8 | Q08775 | Q5T802 |
| <i>Runx2a</i> (MRIPV) | 1152 (partial) | 95.41% | 68.86% | 71.37% | 71.37% |
| GenBank ID: AB274885 | | Q596E7 | A1YIX9 | Q08775 | Q5T802 |
| <i>Runx2b</i> (MASNS) | 678 (partial) | 95.10% | 72.17% | 53.06% | 56.43% |
| GenBank ID: AB274886 | | Q6TYZ4 | A1YIX9 | Q08775 | Q5T802 |
| <i>Runx2b</i> (MRIPV) | 928 (partial) | 97.84% | 76.98% | 86.36% | 86.36% |
| GenBank ID: AB274887 | | Q4VW83 | A1YIX9 | Q08775 | Q5T802 |
| <i>Osterix</i> | 2064 (full) | 86.83% | 50.86% | 62.18% | 64.56% |
| GenBank ID: AB274888 | | Q6U1J4 | A6H8I6 | Q2KHK9 | Q8TDD2 |
| RANKL | 725 (partial) | – | 32.89% | 26.99% | 26.38% |
| GenBank ID: AB459540 | | – | Q5HZR8 | Q059M3 | O14788 |
| Type I collagen | 399 (partial) | 97.74% | 85.71% | 84.21% | 82.71% |
| GenBank ID: AB685219 | | Q6P4U1 | Q9IB91 | Q99LL6 | D3DTX7 |
| ALP | 2391 (full) | 87.86% | 76.08% | 76.29% | 77.11% |
| GenBank ID: AB459538 | | F1Q5B5 | Q32NT2 | Q8JZS4 | B7Z4Y6 |
| Osteocalcin | 469 (full) | 72.12% | 29.13% | 31.68% | 28.71% |
| GenBank ID: AB685220 | | Q4G6A6 | P40147 | P86546 | P02818 |
| NFATc1 | 2544 (partial) | 93.13% | 62.38% | 62.09% | 61.80% |
| GenBank ID: AB685221 | | Q19AW4 | Q6GNH6 | Q6P7T9 | B5B2M |

Each accession number (UniProt ID) of the compared amino acid sequence is written one line below the percent homology.

Histological evidence of scale resorption and new scale formation

On day 5, transplantation in methanol-fixed and proteinase K-treated scales triggered apparent inflammation, bleeding, and edema in and around the transplant areas; the same was observed in polarity reversal (upside-down) scales, but with less inflammation. TRAP staining on day 5 indicated that osteoclastic activities in the methanol-fixed, the proteinase K-treated, and polarity reversal scales (Figs. 2A–C) were higher than those in the sham transplanted and ontogenic scales (Figs. 2D–E). Microscopically, the numbers of TRAP-positive cells were confirmed to be higher as well. The TRAP-positive area on scale increased with time (Table 3). On day 15, many multinucleated osteoclasts appeared (Fig. 3C), and the methanol-fixed and proteinase K-treated transplants were resorbed (Fig. 3B). Post-transplant new scale formation was found since day 10 on the posterior side of every modified transplanted scale, including methanol-fixed transplants (Fig. 2F), proteinase K-treated cell-free transplants (Fig. 2G), and the polarity reversal (upside-down) transplants (Fig. 2H). The new scales were positively stained with alkaline phosphatase. Each new scale began to adhere firmly to the posterior side of the transplant and grew larger on day 15. However, the shapes of these scales were not identical to those of spontaneously regenerating scales, and their sizes were smaller when compared with the same-age spontaneously regenerating scales. No new scale regenerated in the sham transplants (Fig. 2I). The sham transplants were well sustained in the scale pockets and were negative for TRAP and ALP staining on days 5 and 10 (Figs. 2D, I). In U-shape trimmed transplants (Figs. 4A–B) and circular-hole perforated transplants (Figs. 4C–F), new scales regenerated at the trimmed and perforated parts of each scale, respectively. In these two groups, scale resorption occurred apparently only around the trimmed/perforated part without obvious inflammation.

Osteoclastic and osteoblastic activities in post-autotransplant methanol-fixed scales and proteinase K-treated scales

At the early post-autotransplant stage (days 3), the mRNA expression amount of early osteoclastic marker NFATc1 in both groups of modified transplanted scales (methanol-fixed transplants and proteinase K-treated transplants) was significantly higher than that in

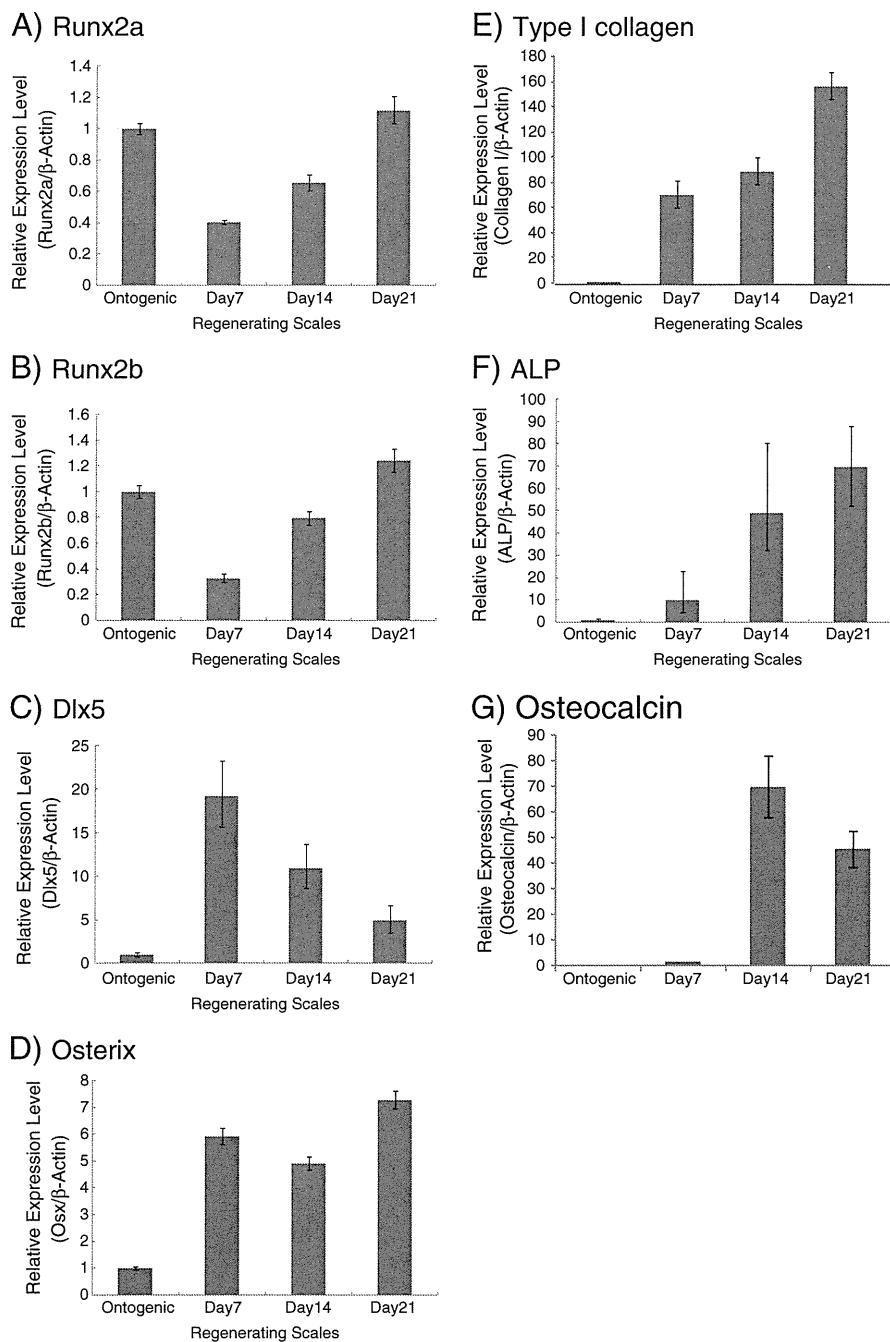


Fig. 1. (A–G). Expression patterns of osteoblastic markers during spontaneous scale regeneration compared to ontogenic scales. Column and bars represent the mean and SEM (N=5), respectively.

the sham transplants and the ontogenic scales ($P < 0.05$) (Fig. 5A), whereas no significant increase in expression of early osteoblastic marker *dlx5*, *osterix* (Figs. 5D–E), and *runx2* (data not shown) was found. In addition, the methanol-fixed transplants and the proteinase K-treated transplant showed slightly higher, but insignificant, levels of *cathK* and *RANKL* (Figs. 5B–C). On the other hand, at the late post-autotransplant stage (days 15), two osteoclastic markers, *TRAP* and *cathK*, and two osteoblastic markers, *collagen I* and *osteocalcin*, in both methanol-fixed transplants and proteinase K-treated transplants were significantly higher when compared to sham autotransplants and ontogenic scales ($P < 0.05$) (Figs. 6A–D). At this stage, no significant result was found in the mRNA expression analysis of *NFATc1* (data not shown).

Discussion

For studying the bone metabolism, using goldfish scale is a simple, cost-effective, and time-saving approach. A goldfish has a total of more than one hundred scales on both sides of its body. Numerous scales can be pulled out at any time without fatal consequences. This condition enables *in vivo* experiments to investigate various stages of the osteo-regeneration process in real-time in the same animal. Moreover, from the same goldfish, harvested scales can be applied by several scale treatments/modifications *in vitro*. For example, scales are divided into several groups, and each group is then treated differently depending on the experimental plan. This opens possibilities for more complex experimental designs. The effects of multiple environment factors can

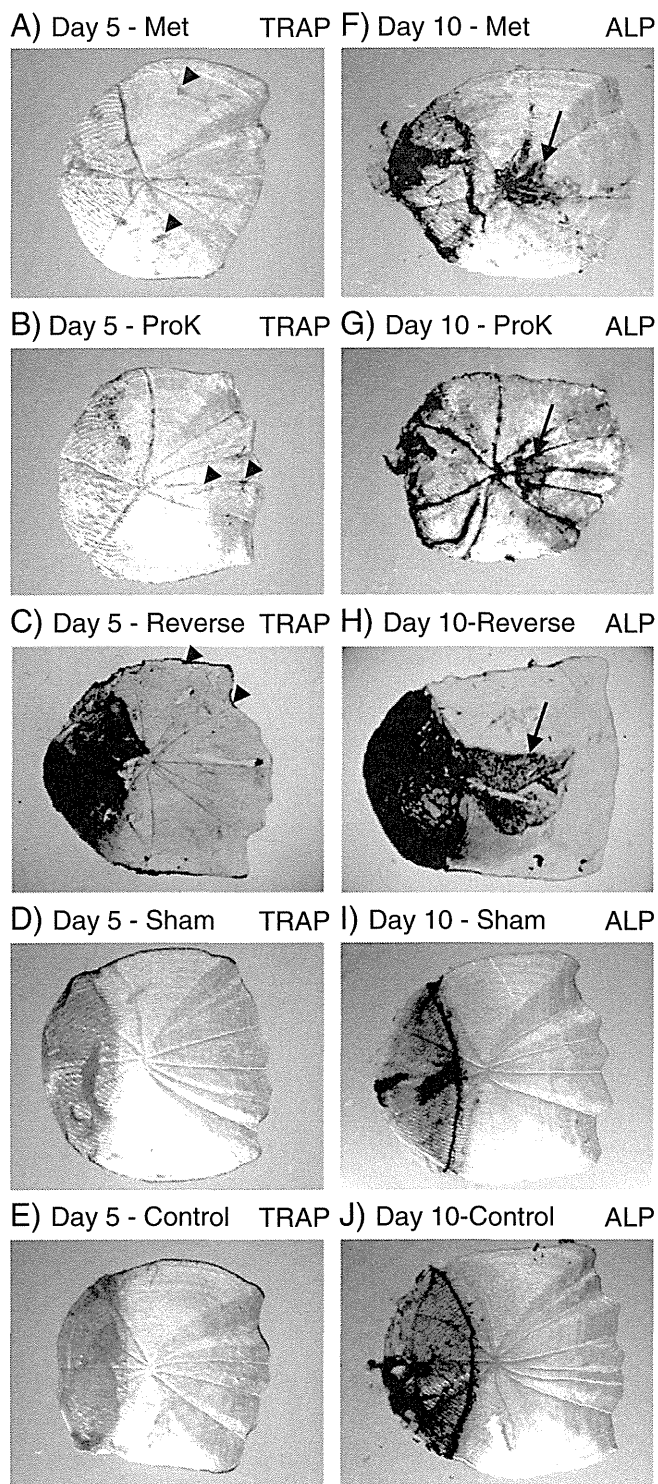


Fig. 2. (A–J). Micrographs of methanol-fixed transplants (Met), proteinase K-treated transplants (ProK), polarity reversal (upside-down) transplants (Reverse), sham transplant (Sham), and ontogenic scales (Control) on day 5 (TRAP staining) and day 10 (ALP staining). Black arrowheads and black arrows indicate the TRAP-positive area and regenerating scales, respectively.

be studied in the same animal. In addition, compared to observing real-time bone regeneration, which requires a high-effort approach such as x-ray irradiation, scales are easier to work with, as they are on the outer part the animal's body.

Our previous histological observation indicated that scale regeneration is very similar to the development of mammalian membrane

Table 3
Summary of the histological observation.

| Type of autotransplant | New scale formation | Scale resorption (osteoclastic activity) | | | |
|-----------------------------------|---------------------|--|-------|--------|--------|
| | | Day 3 | Day 5 | Day 10 | Day 15 |
| Methanol-fixed scale (Met) | ○ | +/- | + | ++ | +++ |
| Proteinasek-treated scale (ProK) | ○ | +/- | + | ++ | +++ |
| Polarity-reversal scale (Reverse) | ○ | +/- | + | + | ++ |
| Unmodified scale (Sham) | — | +/- | — | — | — |

Degree of TRAP-positive area on scales was quantified by numbers of plus signs (+).

bone [2]. Moreover, we reported that the estrogen receptor is expressed in regenerating scales and estrogen participates in osteogenesis as it does in mammalian bone [2]. Genetically, considering the peak and sequence of osteoblastic gene expression, our results are in accordance with those reported in the femoral marrow ablation model [39–41], a conventional model of intramembranous bone

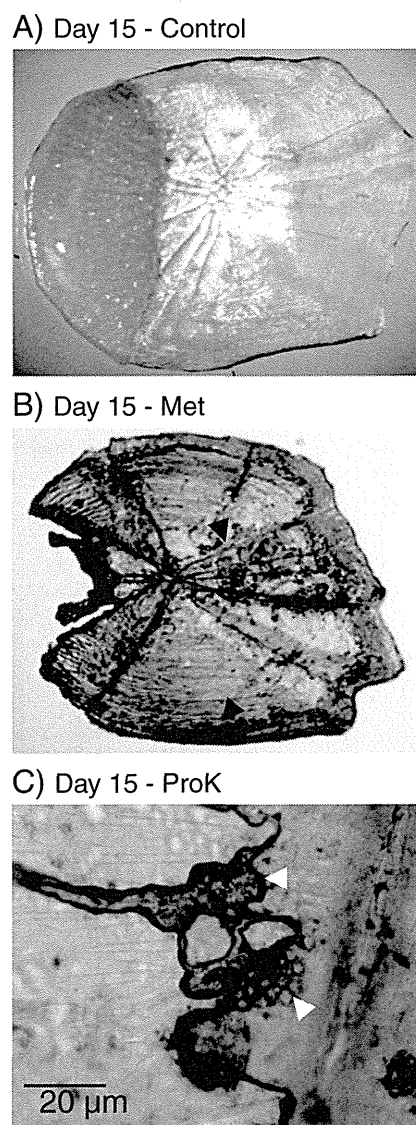


Fig. 3. (A–C). Micrographs of ontogenic scales (Control), methanol-fixed transplants (Met), and proteinase K-treated transplants (ProK) at day 15 after TRAP staining. Black arrowheads and white arrowheads indicate the TRAP-positive area and multi-nucleate osteoclasts, respectively. In panel B, a micrograph was taken after removing the new regenerating scale from the autotransplant. TRAP staining was performed before the removal.

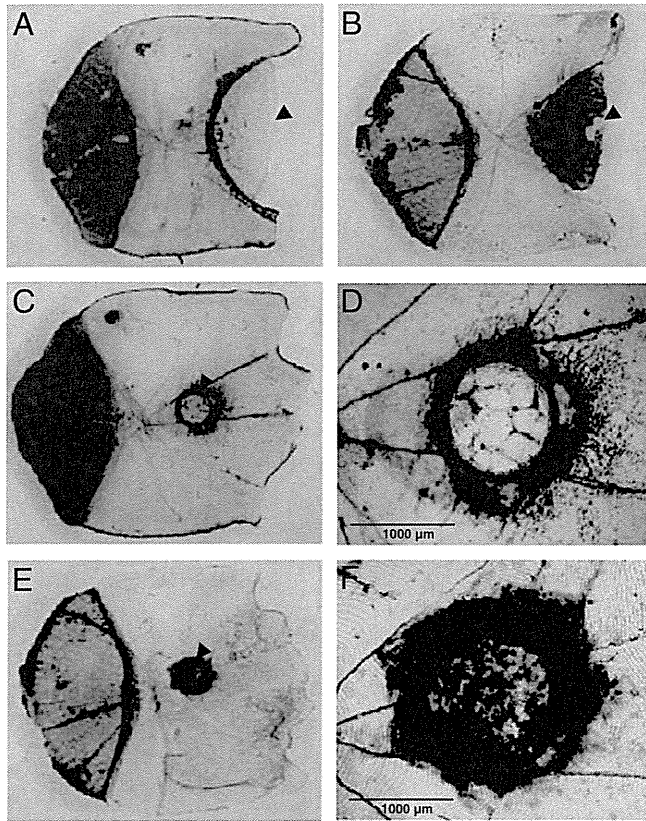


Fig. 4. (A–F). Micrographs of new regenerating scales that formed and adhered to the posterior side of the modified scales at post-autotransplant day 10; U-shape trimmed scales (A–B), circular-hole perforated scales (C, E), and zoom image of C and E (D, F). Each transplant was individually stained with TRAP (A, C, D) and ALP (B, E, F). Black arrowheads indicate new regenerating scales.

regeneration. Scale osteoblastic genes, *dlx5*, *osterix*, collagen, ALP, and osteocalcin, show almost the same patterns of expression as intramembranous bone regeneration. In addition, compared to the results from an *in vitro* experiment using MC3T3-E1 cells [48], scale osteoblastic genes share almost the same sequence of expression except for one gene, *Runx2*. *Runx2* in regenerated scales did not show significant expression above those in ontogenic scales.

In mammal, osteogenesis is regulated by the transcription factors *runx2*, *osterix*, *dlx5*, and *msx2* and the transcriptional activator β -catenin [49]. *Runx2* controls the expression of major osteoblast proteins, such as alkaline phosphatase, collagen, and osteocalcin [20,49]. *Osterix* lies downstream of *runx2* and is necessary for the differentiation of pre-osteoblasts into mature osteoblasts [49]. *Dlx5* is a homeobox domain transcription factor that also regulates osteogenesis [20,50,51] and is involved in the response of osteogenic cells to BMP-2 [21,52,53]. In the present study, both transcription factor *dlx5* and *osterix* were found to be expressed during scale regeneration prior to activation of the osteoblast functional genes type I collagen, ALP, and osteocalcin (Figs. 1C–G). These results indicate that genetic regulation of scale regeneration resembles that of developing mammalian bone. In mammals, *runx2* is the first osteoblast-specific transcription factor to be identified and still the earliest cell-specific transcription determinant known in this cell lineage [54]. Many molecular biology, mouse, and human genetic studies converge to demonstrate that *runx2* is a master gene of osteoblast differentiation [55]. However, our present study indicated that *runx2* is less likely to be a crucial factor in an early stage of scale regeneration, while *dlx5* is rather contributory for the following reasons: 1) *runx2* mRNA during the early stage of scale regeneration did not show significant expression above those in ontogenic scales (Figs. 1A–B), while *dlx5* did (Fig. 1C), and 2) in the same sample, the

cycle threshold of *dlx5* (CT value = 27–28) was lower than that of *runx2* (CT value = 31–32), indicating that *dlx5* mRNA expression was much higher than *runx2*.

For osteoclasts, it has been shown that scale osteoclasts and bone osteoclasts share elements morphologically and genetically. Scale osteoclasts create a ruffled border which is rich in mitochondria to increase the surface area interface for bone resorption. Mature scale osteoclasts are multinucleated and express TRAP and cathK [1]. Together with scale osteoblasts, scale osteoclasts respond to parathyroid hormone 1 (1–34) [10]. In bone, osteoclasts are differentiated from hemopoietic precursor cells at bone-resorbing sites under the control of osteotropic hormones and local factors produced in the microenvironment [56–58]. Nonetheless, to the best of our knowledge, the specific location where goldfish scale osteoclasts differentiate is unknown. In this study, the presence of early osteoclastic markers (NFATc1 and RANKL) in cell-free autotransplants on day 3 indicates that early (undifferentiated) osteoclasts did migrate to the autotransplants. After this, elevation of late osteoclastic markers (TRAP and cathK) was detected (Figs. 6A–B). This result indicates that differentiation of scale osteoclast is most likely taking place in autotransplants.

We consider that the regeneration of scale after scale injury can be used as a model for studying bone regeneration. For example, from an autotransplantation experiment, the regeneration process in U-shape trimmed scales and circular-hole perforated scales could resemble the healing process in a bone fracture. Besides, the regeneration process in polarity reversal (upside-down) scales and cell-free scales may be a model for bone regeneration after inflammation. In the present study, we found that new scales regenerated at the trimmed/perforated part of each transplant without obvious inflammation (Figs. 4A–B: U-shape trimmed transplants and Figs. 4C–F: circular-hole perforated transplants). However, inflammation is another considerable possibility that could induce the onset of scale resorption and regeneration. The inflammation-induced bone resorption theory reviewed in [59] could be used to explain the process. Briefly, several cytokines and inflammatory mediators have been shown to be able to stimulate osteoclast formation and bone resorption and have, therefore, been implicated in the pathogenesis of inflammation-induced bone resorption. Some cytokines, the two kinins bradykinin and kallidin, as well as thrombin, are stimulatory, whereas other cytokines are inhibitory. Stimulatory cytokines exert their effects not by affecting the osteoclast progenitor cells directly but by stimulating the RANKL/OPG ratio in periosteal osteoblasts. Inhibitory cytokines cause their effects either indirectly, by affecting osteoblasts, or, in some cases, directly, by affecting the osteoclast progenitor cells. Chemokines are important for the recruitment of osteoclast progenitor cells to the inflammatory site and also for the fusion of these cells to multi-nucleated osteoclasts. In the current study, we found that RANKL expression increased in the early stage of all modified scale autotransplants. However, at this stage, the expression of osteoblastic markers *dlx5* and *osterix* was still insignificant. To explain this point, it is possible that the cells that expressed RANKL could be cells other than osteoblasts, such as those involved in the inflammatory response. Lymphocytes, fibroblasts, inflammatory epithelial cells and synovial cells have been reported to express RANKL [60–65].

In our scale transplant model, we entirely disrupted the spontaneous cell-to-cell contact between the scale-pocket lining and scale cortex in groups 1–3 by pulling off the scales, modifying them (by methanol-fixation, proteinase K-treatment, and polarity reversal (upside-down)), and re-inserting them into their original scale pockets. Similarly, we partially disrupted the cell-to-cell contact in groups 4–5 by U-shape trimming and circular-hole perforation. Here, we demonstrated that correct cell-to-cell contact between the scale-pocket lining cells and scale cortex cells is the key to switch off the onset of scale resorption and regeneration. Sham transplantation was the only method that did not produce a result in scale resorption and new scale formation. This could be explained by the fact that the reported method had caused the scale pocket lining to be disconnected from the scale surface for only a short

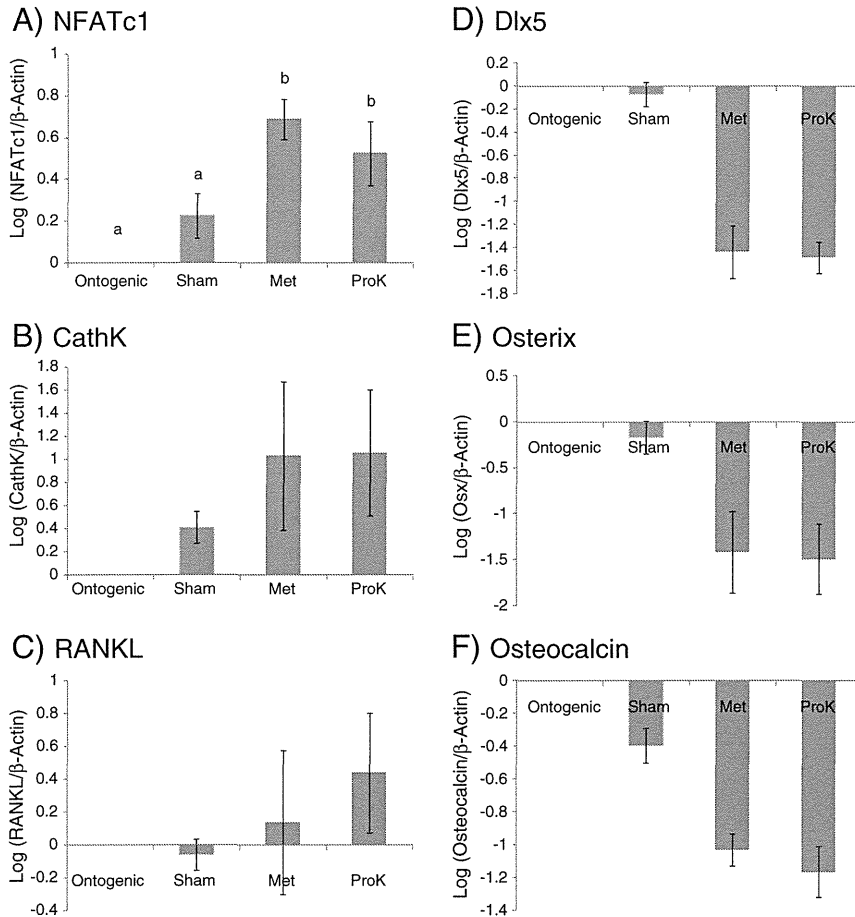


Fig. 5. (A–F). Relative expression amounts of osteoclastic and osteoblastic marker mRNA in methanol-fixed transplants (Met), proteinase K-treated transplants (ProK), and sham transplants on day 3 compared to those in ontogenic scales. Column and bars represent the mean and SEM (N = 5), respectively. The different superscripts represent statistically significant differences at P < 0.05.

time (about 5–10 s). This enabled the post-transplant revascularization and made it possible for the old cell-to-cell contact to be preserved. On the contrary, it was difficult for the old cell-to-cell contact to be correctly

re-established in the methanol-fixed transplant, proteinase K-treated cell-free transplant, and polarity reversal (upside-down) transplant. In these groups, resorption of the transplanted scales took place first, and

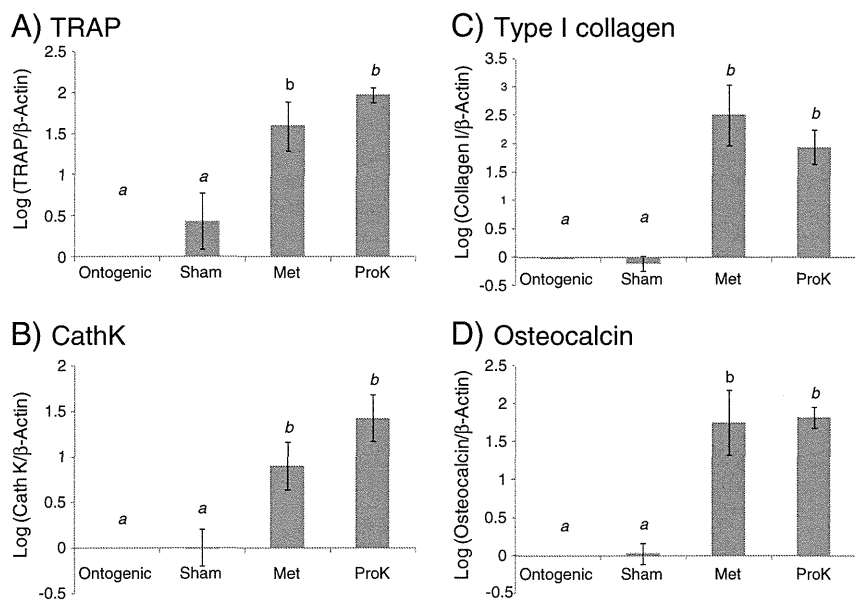


Fig. 6. (A–D). Relative expression amounts of osteoclastic and osteoblastic marker mRNA in methanol-fixed transplants (Met), proteinase K-treated transplants (ProK), and sham transplants in the late post-autotransplant stage (day 15) compared to those in ontogenic scales. Column and bars represent the mean and SEM (N = 5), respectively. The different superscripts represent statistically significant differences at P < 0.05.

new scale regeneration followed. Again, we found that scale regeneration started at the area that lacks cell-to-cell contact (trimmed/perforated parts) in transplant groups 4–5. From our preliminary experiments, trimmed/perforated scales could not be regenerated *in vitro* when cultured without scale pocket tissue. With scale pocket tissue, however, the new scale regenerated at the trimmed/perforated parts but had not fully grown. This may be due to the other environmental conditions. From these facts, we suggest that the preserved cell-to-cell contact should be considered to be a determining factor for inhibiting scale resorption and formation.

As for the loss of cell-to-cell contact theory, similar to our results, it has been shown that the proliferation of type 1 astrocytes is strongly inhibited by homotypic cell contact [66]. In addition, the cell-to-cell contact-dependent inhibition of astrocyte proliferation and reactive gliosis was demonstrated *in vitro* and *in vivo* [67]. In this process, cyclin-dependent kinase P27 contributes to the regulation of cell cycle re-entry in type 1 astrocytes [67,68]. In liver regeneration as well, hepatocytes can also be primed to respond to the hepatocyte growth factor and transforming growth factor alpha by mild collagenase perfusion of intact liver, suggesting that the loss of cell-to-cell contact may facilitate re-entry into the cell cycle [69]. Moreover, even though it is not well understood, loss of cell-to-cell contact is suggested to be an important early regulator of intestinal regeneration by being a potential modulator in initiating signal and cell proliferation [70]. In the present study, correct cell-to-cell contact withheld scale resorption in sham transplantation, as shown in Table 3; TRAP positive disappeared after day 5. On the contrary, in the methanol-fixed (scale with non-living cells) and proteinase K-treated (cell-free scale) transplants, scale resorption preceded new scale formation and lasted at least until two weeks after transplantation. Our experiment is the first to show that, other than induce cell proliferation, loss of cell-to-cell contact could trigger the resorption process. In addition, the resorption process was confirmed to happen before the regeneration process.

In conclusion, we found that goldfish scale regeneration shares similarities in gene expression and morphology with intramembranous bone regeneration. Using scale regeneration as a model of intramembranous bone regeneration has advantages over the conventional bone marrow ablation model, largely because it does not require that animal be sacrificed. Moreover, the goldfish scale regeneration model allows all stages of the regeneration process to be observed in the same animal. Improved understanding of scale regeneration will help elucidate the process of intramembranous bone regeneration. Therefore, we consider goldfish scale as a possible new tool to study intramembranous bone regeneration.

Acknowledgments

This study was supported in part by grants to A.H. (Grant-in-Aid for Scientific Research (C) No. 21570062 by JSPS) and to N.S. (Grant-in-Aid for Scientific Research (C) No. 21500404 by JSPS; Grant-in-Aid for Space Utilization by Japan Aerospace Exploration Agency; the Environment Research and Technology Development Fund (B-0905) by the Ministry of the Environment in Japan; Health and Labour Sciences Research Grants of Ministry of Health, Labour and Welfare, Japan).

References

- [1] Azuma K, Kobayashi M, Nakamura M, Suzuki N, Yashima S, Iwamura S, et al. Two osteoclastic markers expressed in multinucleate osteoclasts of goldfish scales. *Biochem Biophys Res Commun* 2007;362:594–600.
- [2] Yoshikubo H, Suzuki N, Takemura K, Hoso M, Yashima S, Iwamura S, et al. Osteoblastic activity and estrogenic response in the regenerating scale of goldfish, a good model of osteogenesis. *Life Sci* 2005;76:2699–709.
- [3] Suzuki N, Kitamura K, Nemoto T, Shimizu N, Wada S, Kondo T, et al. Effect of vibration on osteoblastic and osteoclastic activities: analysis of bone metabolism using goldfish scale as a model for bone. *Adv Space Res* 2007;40:1711–21.
- [4] Suzuki N, Somei M, Seki A, Reiter RJ, Hattori A. Novel bromomelanin derivatives as potentially effective drugs to treat bone diseases. *J Pineal Res* 2008;45:229–34.
- [5] Ejiri S. The preosteoclast and its cytodifferentiation into the osteoclast: ultrastructural and histochemical studies of rat fetal parietal bone. *Arch Histol Jpn* 1983;46:533–57.
- [6] Komori T, Yagi H, Nomura S, Yamaguchi A, Sasaki K, Deguchi K, et al. Targeted disruption of *Cbfa1* results in a complete lack of bone formation owing to maturational arrest of osteoblasts. *Cell* 1997;89:755–64.
- [7] Rice DP, Rice R, Thesleff I. Molecular mechanisms in calvarial bone and suture development, and their relation to craniosynostosis. *Eur J Orthod* 2003;25:139–48.
- [8] Lian JB, Balint E, Javed A, Drissi H, Vittori R, Quinlan EJ, et al. Runx1/AML1 hematopoietic transcription factor contributes to skeletal development *in vivo*. *J Cell Physiol* 2003;196:301–11.
- [9] Ito Y, Yeo JY, Chytil A, Han J, Bringas Jr P, Nakajima A, et al. Conditional inactivation of *Tgfb2* in cranial neural crest causes cleft palate and calvaria defects. *Development* 2003;130:5269–80.
- [10] Suzuki N, Danks JA, Maruyama Y, Ikegame M, Sasayama Y, Hattori A, et al. Parathyroid hormone 1 (1–34) acts on the scales and involves calcium metabolism in goldfish. *Bone* 2011;48:1186–93.
- [11] Witten PE, Bendahmane M, Abou-Haila A. Enzyme histochemical characteristics of osteoblasts and mononucleated osteoclasts in a teleost fish with acellular bone (*Oreochromis niloticus*, Cichlidae). *Cell Tissue Res* 1997;287:591–9.
- [12] Flores M, Tsang V, Hu W, Kaley-Zylinska M, Postlethwait J, Crosier P, et al. Duplicate zebrafish *runx2* orthologues are expressed in developing skeletal elements. *Gene Expr Patterns* 2004;4:573–81.
- [13] Glenney GW, Wiens GD. Early diversification of the TNF superfamily in teleosts: genomic characterization and expression analysis. *J Immunol* 2007;178:7955–73.
- [14] Zylberberg L, Bonaventure J, Cohen-Solal L, Hartmann D, Bereiterhahn J. Organization and characterization of fibrillar collagens in fish scales *in situ* and *in vitro*. *J Cell Sci* 1992;103:273.
- [15] Renn J, Winkler C. Osterix-mCherry transgenic medaka for *in vivo* imaging of bone formation. *Dev Dyn* 2009;238:241–8.
- [16] Gavaia PJ, Simes DC, Ortiz-Delgado JB, Viegas CS, Pinto JP, Kelsh RN, et al. Osteocalcin and matrix Gla protein in zebrafish (*Danio rerio*) and Senegal sole (*Solea senegalensis*): comparative gene and protein expression during larval development through adulthood. *Gene Expr Patterns* 2006;6:637–52.
- [17] Pinto JP, Conceicao N, Gavaia PJ, Cancela ML. Matrix Gla protein gene expression and protein accumulation colocalize with cartilage distribution during development of the teleost fish *Sparus aurata*. *Bone* 2003;32:201–10.
- [18] Aubin JE, Gupta AK, Bhargava U, Turksen K. Expression and regulation of galectin 3 in rat osteoblastic cells. *J Cell Physiol* 1996;169:468–80.
- [19] Nishimoto SK, Araki N, Robinson FD, Waite JH. Discovery of bone gamma-carboxyglutamic acid protein in mineralized scales. The abundance and structure of *Lepomis macrochirus* bone gamma-carboxyglutamic acid protein. *J Biol Chem* 1992;267:11600–5.
- [20] Li H, Marijanovic I, Kronenberg MS, Erceg I, Stover ML, Velonis D, et al. Expression and function of *Dlx* genes in the osteoblast lineage. *Dev Biol* 2008;316:458–70.
- [21] Lee MH, Kim YJ, Kim HJ, Park HD, Kang AR, Kyung HM, et al. BMP-2-induced *Runx2* expression is mediated by *Dlx5*, and TGF-beta 1 opposes the BMP-2-induced osteoblast differentiation by suppression of *Dlx5* expression. *J Biol Chem* 2003;278:34387–94.
- [22] Harris SE, Guo D, Harris MA, Krishnaswamy A, Lichtler A. Transcriptional regulation of BMP-2 activated genes in osteoblasts using gene expression microarray analysis: role of *Dlx2* and *Dlx5* transcription factors. *Front Biosci* 2003;8:s1249–65.
- [23] Verreijdt L, Debais-Thibaud M, Borday-Birraux V. Expression of the *dlx* gene family during formation of the cranial bones in the zebrafish (*Danio rerio*): differential involvement in the visceral skeleton and braincase. *Dev Dyn* 2006;235:1371–89.
- [24] Abe G, Ide H, Tamura K. Function of FGF signaling in the developmental process of the median fin fold in zebrafish. *Dev Biol* 2007;304:355–66.
- [25] Sire JY. The same cell lineage is involved in scale formation and regeneration in the teleost fish *Hemichromis bimaculatus*. *Tissue Cell* 1989;21:447–62.
- [26] Squier C, Ghoneim S, Kremnak C. Ultrastructure of the periosteum from membrane bone. *J Anat* 1990;171:233.
- [27] Fell H. The osteogenic capacity *in vitro* of periosteum and endosteum isolated from the limb skeleton of fowl embryos and young chicks. *J Anat* 1932;66:157.
- [28] Ito Y, Fitzsimmons J, Sanyal A, Mello M, Mukherjee N, O'driscoll S. Localization of chondrocyte precursors in periosteum. *Osteoarthritis Cartilage* 2001;9:215–23.
- [29] Dwek JR. The periosteum: what is it, where is it, and what mimics it in its absence? *Skeletal Radiol* 2010;39:319–23.
- [30] Sire JY, Géraudie J. Fine structure of regenerating scales and their associated cells in the cichlid *Hemichromis bimaculatus* (Gill). *Cell Tissue Res* 1984;237:537–47.
- [31] Neave F. On the histology and regeneration of the teleost scale. *Q J Microsc Sci NS* 1940;81:541–68.
- [32] Zhao Q, Wang X, Liu Y, He A, Jia R. NFATc1: functions in osteoclasts. *Int J Biochem Cell Biol* 2010;42:576–9.
- [33] DR S.. Fixation of implants. In: Callaghan JJ, Rosenberg AG, Rubash HE, Simonian PT, Wickiewicz TA, editors. *The adult knee*. Philadelphia: Lippincott Williams & Wilkins; 2003. p. 289–96.
- [34] Amsel S, Maniatis A, Tavassoli M, Crosby WH. The significance of intramedullary cancellous bone formation in the repair of bone marrow tissue. *Anat Rec* 1969;164:101–11.
- [35] Patt HM, Maloney MA. Bone marrow regeneration after local injury: a review. *Exp Hematol* 1975;3:135–48.
- [36] Liang CT, Barnes J, Seedor JG, Quartuccio HA, Bolander M, Jeffrey JJ, et al. Impaired bone activity in aged rats: alterations at the cellular and molecular levels. *Bone* 1992;13:435–41.

- [37] Suva LJ, Seedor JG, Endo N, Quartuccio HA, Thompson DD, Bab I, et al. Pattern of gene expression following rat tibial marrow ablation. *J Bone Miner Res* 1993;8:379–88.
- [38] Bab IA. Postablation bone marrow regeneration: an *in vivo* model to study differential regulation of bone formation and resorption. *Bone* 1995;17:437S–41S.
- [39] Lu H, Kraut D, Gerstenfeld LC, Graves DT. Diabetes interferes with the bone formation by affecting the expression of transcription factors that regulate osteoblast differentiation. *Endocrinology* 2003;144:346–52.
- [40] Boabaid F, Berry JE, Koh AJ, Somerman MJ, McCauley LK. The role of parathyroid hormone-related protein in the regulation of osteoclastogenesis by cementoblasts. *J Periodontol* 2004;75:1247–54.
- [41] Kuroda S, Viridi AS, Dai Y, Shott S, Sumner DR. Patterns and localization of gene expression during intramembranous bone regeneration in the rat femoral marrow ablation model. *Calcif Tissue Int* 2005;77:212–25.
- [42] van der Meulen T, Kranenbarg S, Schipper H, Samallo J, van Leeuwen JL, Franssen H. Identification and characterisation of two runx2 homologues in zebrafish with different expression patterns. *Biochim Biophys Acta* 2005;1729:105–17.
- [43] Suzuki N, Hattori A. Melatonin suppresses osteoclastic and osteoblastic activities in the scales of goldfish. *J Pineal Res* 2002;33:253–8.
- [44] Milona M, Gough J, Edgar A. Expression of alternatively spliced isoforms of human Sp7 in osteoblast-like cells. *BMC Genomics* 2003;4:43.
- [45] Weiss MJ, Henthorn PS, Lafferty MA, Slaughter C, Raducha M, Harris H. Isolation and characterization of a cDNA encoding a human liver/bone/kidney-type alkaline phosphatase. *Proc Natl Acad Sci* 1986;83:7182.
- [46] Dohi Y, Tabata S, Yamaguchi M, Ohgushi H, Yonemasu K. Characterization of the cDNA encoding bullfrog, *Rana catesbeiana*, osteocalcin and two forms of the protein isolated from bone*. *Biochimie* 2004;86:471–80.
- [47] Nishimoto SK, Waite JH, Nishimoto M, Kriwacki RW. Structure, activity, and distribution of fish osteocalcin. *J Biol Chem* 2003;278:11843.
- [48] Maeda T, Matsunuma A, Kurahashi I, Yanagawa T, Yoshida H, Horiuchi N. Induction of osteoblast differentiation indices by statins in MC3T3-E1 cells. *J Cell Biochem* 2004;92:458–71.
- [49] Komori T. Regulation of osteoblast differentiation by transcription factors. *J Cell Biochem* 2006;99:1233–9.
- [50] Lee M, Kim Y, Yoon W, Kim J, Kim B, Hwang Y, et al. Dlx5 specifically regulates Runx2 type II expression by binding to homeodomain-response elements in the Runx2 distal promoter. *J Biol Chem* 2005;280:35579–87.
- [51] Samee N, Geoffroy V, Marty C, Schiltz C, Vieux-Rochas M, Levi G, et al. Dlx5, a positive regulator of osteoblastogenesis, is essential for osteoblast-osteoclast coupling. *Am J Pathol* 2008;173:773–80.
- [52] Lee MH, Kwon TG, Park HS, Wozney JM, Ryoo HM. BMP-2-induced Osterix expression is mediated by Dlx5 but is independent of Runx2. *Biochem Biophys Res Commun* 2003;309:689–94.
- [53] Ulsamer A, Ortuño M, Ruiz S, Susperregui A, Osses N, Rosa J, et al. BMP-2 induces Osterix expression through up-regulation of Dlx5 and its phosphorylation by p38. *J Biol Chem* 2008;283:3816–26.
- [54] Ducey P, Zhang R, Geoffroy V, Ridall AL, Karsenty G. Osf2/Cbfa1: a transcriptional activator of osteoblast differentiation. *Cell* 1997;89:747–54.
- [55] Karsenty G, Kronenberg H, Settembre C. Genetic control of bone formation. *Annual Review of Cell and Developmental* 2009;25:629–48.
- [56] Suda T, Takahashi N, Martin TJ. Modulation of osteoclast differentiation. *Endocr Rev* 1992;13:66–80.
- [57] Suda T, Udagawa N, Nakamura I, Miyaura C, Takahashi N. Modulation of osteoclast differentiation by local factors. *Bone* 1995;17:87S–91S.
- [58] Roodman GD. Advances in bone biology: the osteoclast. *Endocr Rev* 1996;17:308–32.
- [59] Lerner UH. Inflammation-induced bone remodeling in periodontal disease and the influence of post-menopausal osteoporosis. *J Dent Res* 2006;85:596–607.
- [60] Romas E, Gillespie MT, Martin TJ. Involvement of receptor activator of NfκappaB ligand and tumor necrosis factor-α in bone destruction in rheumatoid arthritis. *Bone* 2002;30:340–6.
- [61] Weitzmann MN, Pacifici R. The role of T lymphocytes in bone metabolism. *Immunol Rev* 2005;208:154–68.
- [62] Quinn JM, Gillespie MT. Modulation of osteoclast formation. *Biochem Biophys Res Commun* 2005;328:739–45.
- [63] Romas E, Bakharevski O, Hards DK, Kartsogiannis V, Quinn JM, Ryan PF, et al. Expression of osteoclast differentiation factor at sites of bone erosion in collagen-induced arthritis. *Arthritis Rheum* 2000;43:821–6.
- [64] Martin TJ, Gillespie MT. Receptor activator of nuclear factor [κ] B ligand (RANKL): another link between breast and bone. *Trends Endocrinol Metab* 2001;12:2–4.
- [65] Srivastava S, Matsuda M, Hou Z, Bailey JP, Kitazawa R, Herbst MP, et al. Receptor activator of NF-κB ligand induction via Jak2 and Stat5a in mammary epithelial cells. *J Biol Chem* 2003;278:46171.
- [66] Nakatsuji Y, Miller RH. Homotypic cell contact-dependent inhibition of astrocyte proliferation. *Glia* 1998;22:379–89.
- [67] Koguchi K, Nakatsuji Y, Nakayama K, Sakoda S. Modulation of astrocyte proliferation by cyclin-dependent kinase inhibitor p27(Kip1). *Glia* 2002;37:93–104.
- [68] Nakatsuji Y, Miller RH. Density dependent modulation of cell cycle protein expression in astrocytes. *J Neurosci Res* 2001;66:487–96.
- [69] Liu ML, Mars WM, Zarnegar R, Michalopoulos GK. Collagenase pretreatment and the mitogenic effects of hepatocyte growth factor and transforming growth factor-α in adult rat liver. *Hepatology* 1994;19:1521–7.
- [70] Thompson JS, Saxena SK, Sharp JG. Regulation of intestinal regeneration: new insights. *Microsc Res Tech* 2000;51:129–37.